Radiative Transfer of Ultrasound

Joseph A. Turner and Richard L. Weaver
Department of Theoretical and Applied Mechanics
University of Illinois at Urbana-Champaign
Urbana, IL 61801

Abstract

A radiative transfer equation is used to model the diffuse multiple scattering of ultrasound in a medium containing discrete random scatterers. An assumption of uncorrelated phases allows one to write an equation of energy balance for the diffuse intensity. This ultrasonic radiative transfer equation contains single-scattering and propagation parameters that are calculated using the elastic wave equation. Polarization effects are included through the introduction of an elastodynamic Stokes vector which contains a longitudinal Stokes parameter and four shear Stokes parameters similar to the four Stokes parameters used in optical radiative transfer theory. The theory is applied to a statistically homogeneous, isotropic elastic half space containing randomly distributed spherical voids illuminated by a harmonic plane wave. Results on the angular dependence of backscattered intensity are presented. It is anticipated that this approach may be applicable to materials characterization through the study of the time, space, ultrasonic frequency, and angular dependence of diffusely scattered ultrasound in elastic media with microstructure.

INTRODUCTION

Ultrasonic materials characterization of solid media with random microstructures relies, in the literature, mostly upon the use of the coherent field, through measurements of either wave speed or attenuation[1,2,3,4,5]. The modern state of the theory relating microstructure to such wave properties may be found in Stanke and Kino[6], and Hirsekorn[7] for the case of polycrystalline media, and Twersky[8], Tsang *et al.*[9], and Varadan *et al.*[10] for media consisting of discrete scatterers. The use of the incoherent, or speckle, field for purposes of materials characterization is less well developed. A number of researchers[11,12,13,14,15,16] discuss the use of the incoherently singly backscattered field for microstructural characterization. This literature shows that the singly backscattered waves dominate in the limit that the scattering is sufficiently weak. In the opposite limit Guo *et al.*[17] and Weaver *et al.*[18,19] have discussed and demonstrated the use of the speckle field in the limit in which typical rays have incoherently scattered sufficiently many times that the field may be modeled by a diffusion equation.

The parameter range between these two limits of single and multiple scattering is, though, of great importance. The singly scattered field is sometimes difficult to access experimentally in media with strong scattering. The multiply scattered field is, additionally, sensitive to scattering amplitudes in arbitrary directions, and to absorption as well as to scattering[18,20] and therefore contains information not available in the singly scattered field. The few existent attempts to create theories which bridge the gap between these two limits are, to date, limited to rather ad-hoc efforts to model the twice scattered field[20]. In this communication we present a description of the diffuse ultrasonic field throughout the entire parameter range from single scattering to the diffusion limit. The approach is based upon the concepts from Radiative Transfer Theory first developed for the treatment of multiply scattered electromagnetic radiation in stellar and planetary atmospheres[21,22,23].

In the following section we develop the ultrasonic radiative transfer equation (URTE) after an introduction of concepts relevant to its derivation. In section II we discuss the derivation of the single scattering parameters needed in the URTE for the case of spherical scatterers in an elastic medium. In section III we discuss the solution of the URTE and finally present sample results in section IV.

I. RADIATIVE TRANSFER THEORY

When the time and/or length scales in an experiment become long compared to the time and length scales between successive random scatterings of a wave, the modeler must account for multiple scattering of the wave. Radiative transfer theory is an approximate method for the modeling of that multiple scattering. It is based upon an assumption that randomly scattered waves have uncorrelated random phases. The superposition of such waves therefore may be effected incoherently, leading to a description of the wave field, not in terms of field quantities such as stress or material displacement, but in terms of the average intensities. As such it of course cannot be a complete description of the disturbance. One may hope that it is an accurate description, however, of ensemble averaged energy densities[24].

The radiative transfer equation (RTE) may be derived in either of two ways. The simpler phenomenological method relies upon considerations of energy balance in representative volume elements consisting of several scatterers. In this approach the wave equation itself is used only for the determination of propagation speeds and for the determination of the properties of the single scattering events which constitute the multiple scattering process.

One may also derive RTE's directly from the wave equation by consideration of the ensemble average of the covariance of the Green's function in the random medium. Barabanenkov[25] showed this for the case of a scalar medium. Weaver[18], for purposes of deriving the behavior of the field in the diffusion limit, independently used this method for the derivation

of an RTE for elastic wave scattering in a polycrystalline medium consisting of randomly oriented cubic crystallites. The generalization of that RTE and its solution will be the subject of a later communication.

In this section we adapt the phenomenological RTE derivation to the case of an elastic medium containing uncorrelated discrete scatterers. A derivation of the scalar radiative transfer equation is presented in the first subsection in order to clarify the ultrasonic radiative transfer equation derived later. After Stokes parameters are introduced with which to describe diffuse elastic wave intensity, an analogous procedure is then followed for the derivation of the URTE. This RTE has as a parameter a "Mueller" matrix describing the single scattering process - a form for which for spherical scatterers is derived in section II. The section concludes with discussions of integrals of the URTE related to energy conservation, with the form of the URTE in a common simple geometry, and with a discussion of the closed form single scattering solution of the URTE. The reader may consult the works of Chandrasekhar[21], Sobolev[22], Ishimaru[23], van de Hulst[26], and many others for further insight into radiative transfer equations and their derivation.

A. Scalar Radiative Transfer Equation

Consider the elemental volume shown in Figure 1 with cross-section da and length ds containing $\eta da ds$ scatterers with η the number density of scatterers. Let the spatially incoherent intensity be defined as the energy per area, per time, and per solid angle $d\Omega$ so that the energy emergent from this volume in the $\hat{\mathbf{s}}$ direction is $I(s,t)da\,dt\,d\Omega$. The energy a distance ds away, moving at speed c also in the $\hat{\mathbf{s}}$ direction at a time $dt = ds/c$ later will be $I(s+ds, t+dt)da\,dt\,d\Omega$. The difference in energy can be attributed to a loss caused by absorption and scattering, and an increase caused by emissions into the direction of propagation from other scattering events or from sources within the medium. This energy balance is written

$$I(s+ds,t+dt)da\,dt\,d\Omega - I(s,t)da\,dt\,d\Omega = -\eta\sigma I(s,t)da\,ds\,dt\,d\Omega + \eta\varepsilon(s,t)da\,ds\,dt\,d\Omega, \qquad (1)$$

where $\sigma = \upsilon + \kappa$ is the total extinction cross section per scatterer, υ is the absorption cross section per scatterer, κ is the scattering cross section per scatterer, and $\varepsilon(s,t)$ is the emission coefficient per scatter.

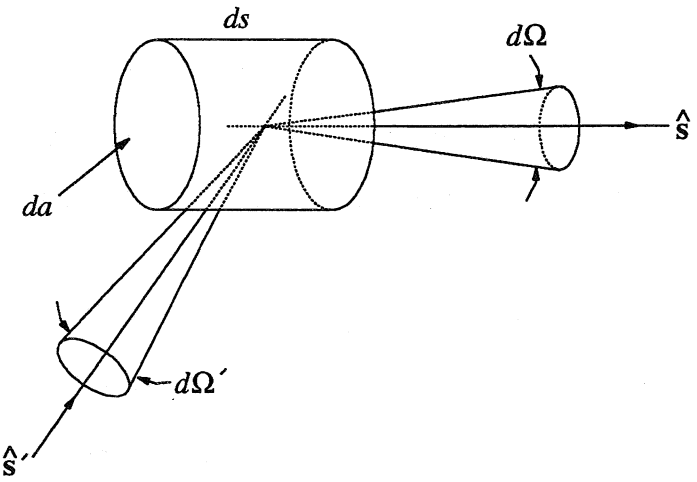

Figure 1. Propagation through the scattering volume in the $\hat{s}$ direction and emission into the $\hat{s}$ direction from scattering events due to energy entering from the $\hat{s}'$ direction.

The absorption cross-section may include absorption within the scatterer as well as dissipation within the medium (which is zero for most applications with electromagnetic waves). The emission coefficient may include emissions from scattering events and primary sources. Eq. (1) implies

$$\frac{\partial I(s,t)}{\partial s}ds + \frac{\partial I(s,t)}{\partial t}dt = -\eta\sigma I(s,t)ds + \eta\varepsilon(s,t)ds. \tag{2}$$

Since $ds = cdt$, Eq. (2) becomes

$$\frac{\partial I(s,t)}{\partial s} + \frac{1}{c}\frac{\partial I(s,t)}{\partial t} = -\eta\sigma I(s,t) + \eta\varepsilon(s,t). \tag{3}$$

Note that in the absence of emissions, I displaces and attenuates with time in the following manner

$$I(s,t) = f(s - ct)e^{-\eta\sigma ct}, \tag{4}$$

which shows that the quantity $\eta\sigma/2$ may be identified with conventional ultrasonic attenuation. In three dimensions the RTE becomes

$$\nabla \cdot \hat{\mathbf{s}} I(\mathbf{r},t,\hat{\mathbf{s}}) + \frac{1}{c}\frac{\partial I(\mathbf{r},t,\hat{\mathbf{s}})}{\partial t} = -\eta\sigma I(\mathbf{r},t,\hat{\mathbf{s}}) + \eta\varepsilon(\mathbf{r},t,\hat{\mathbf{s}}), \tag{5}$$

where $\hat{\mathbf{s}}$ is the direction of propagation, $\mathbf{r}$ is the space vector and the extinction cross section has been assumed isotropic (*i.e.* independent of $\hat{\mathbf{s}}$).

To find the emission coefficient, consider the same volume of scatterers with radiation incident from the $\hat{\mathbf{s}}'$ direction within the solid angle $d\Omega'$ scattering into the $\hat{\mathbf{s}}$ direction in solid angle $d\Omega$ also shown in Figure 1. Let the angular distribution of the scattered portion of the radiation, scattered from the $\hat{\mathbf{s}}'$ direction into the $\hat{\mathbf{s}}$ direction, be defined by

$$p(\hat{\mathbf{s}},\hat{\mathbf{s}}')\frac{d\Omega}{4\pi}, \tag{6}$$

where $p(\hat{\mathbf{s}},\hat{\mathbf{s}}')$ is the *scattering indicatrix*[22] or *phase function*[21] and is 4π times the differential scattering cross-section[23]. The scattering indicatrix is normalized so that

$$\frac{1}{4\pi}\int_{\Omega=4\pi} p(\hat{\mathbf{s}},\hat{\mathbf{s}}')d\Omega = \kappa, \tag{7}$$

which means that for isotropic scattering $p(\hat{\mathbf{s}},\hat{\mathbf{s}}') = \kappa$. This angular distribution multiplied by the intensity and integrated over all incoming directions is the emitted radiation per scatterer. Thus in the absence of primary sources the emission coefficient is

$$\varepsilon(\mathbf{r},t,\hat{\mathbf{s}}) = \frac{1}{4\pi}\int_{\Omega'=4\pi} p(\hat{\mathbf{s}},\hat{\mathbf{s}}')I(\mathbf{r},t,\hat{\mathbf{s}}')d\Omega', \tag{8}$$

and the full scalar RTE is written

$$c\nabla \cdot \hat{\mathbf{s}} I(\mathbf{r},t,\hat{\mathbf{s}}) + \frac{\partial I(\mathbf{r},t,\hat{\mathbf{s}})}{\partial t} + c\eta\sigma I(\mathbf{r},t,\hat{\mathbf{s}}) = \frac{c\eta}{4\pi}\int_{\Omega'=4\pi} p(\hat{\mathbf{s}},\hat{\mathbf{s}}')I(\mathbf{r},t,\hat{\mathbf{s}}')d\Omega'. \tag{9}$$

It is a first order integro-partial differential equation in space, time, and propagation direction. Its solutions are in general nontrivial.

One special case of the scalar RTE, used to model many types of atmospheres, is that of a steady-state, plane-parallel medium shown in Figure 2. The intensity is assumed to be independent of the position coordinates x and y, as well as time, but not independent, in general, of propagation direction.

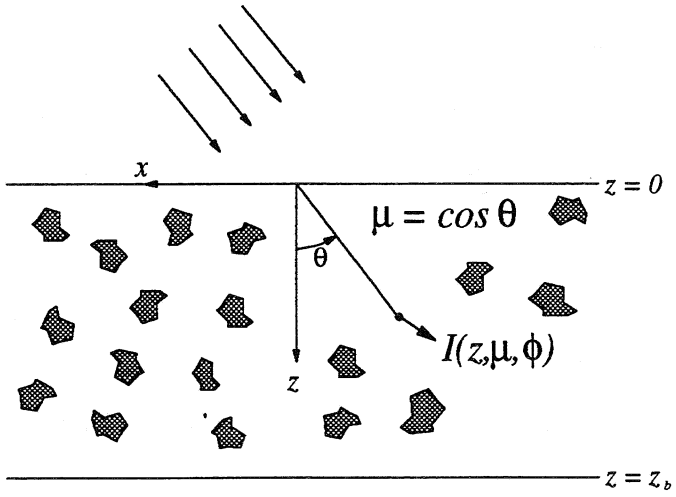

Figure 2. Geometry of a plane-parallel medium.

Under these assumptions, the scalar intensity is a function of position coordinate z only, and the angular variables μ and ϕ, where ϕ is measured from the x axis in a right-hand sense. Under these conditions Eq. (9) simplifies:

$$\mu\frac{\partial I(z,\mu,\phi)}{\partial z} + \eta\sigma I(z,\mu,\phi) = \frac{\eta}{4\pi}\int_0^{2\pi}\int_{-1}^{+1} p(\mu,\phi;\mu',\phi')I(z,\mu',\phi')d\mu'\phi'. \tag{10}$$

If we consider an incident plane wave on the upper surface (z=0) in the (μ_0, ϕ_0) direction with amplitude I_0 and consider no incident radiation on the lower surface (z=z_b), the corresponding boundary conditions are

$$I(z=0,\mu>0,\phi)=I_0\delta(\mu-\mu_0)\delta(\phi-\phi_0), \qquad I(z=z_b,\mu<0,\phi)=0. \tag{11}$$

For a semi-infinite medium we let $z_b \to \infty$.

For a general scattering indicatrix there are no analytical solutions[23] to Eq. (10). Numerical procedures are, however, well developed. The most popular are the method of spherical harmonics[21,27] and the discrete ordinates method[21,23,27].

The scalar radiative transfer equation is adequate for many applications where polarization effects can be neglected such as those dealing with natural light[23]. However, since mode conversion and polarization are important in the elastic case, an examination of the inclusion of polarization through the Stokes vector is necessary.

B. Elastic Stokes Parameters

Characterization of the diffuse ultrasonic intensity requires descriptions of the single longitudinal and both transverse intensities. It is not widely appreciated, however, that a complete characterization will also require description of the degree of phase correlation between the transverse components. Stokes[28] discovered in 1852 that 4 parameters, all with units of intensity, were needed to completely characterize beams of diffuse light. These *Stokes parameters* each propagate independently of the others so that a composite stream of light has Stokes parameters that are the sum of the Stokes parameters of the individual streams. Therefore, a radiative transfer equation can be written for each Stokes parameter. Mode conversion scattering between Stokes parameters may be accounted for within the emission term. For a more detailed explanation of the Stokes parameters see for example Chandrasekhar[21],

Sobolev[22], Ishimaru[23], van de Hulst[26], and Stokes[28]. In this subsection we examine intensity in an elastic solid and introduce five *elastic Stokes parameters*, four for the transverse waves and one for the longitudinal wave.

We consider a time-harmonic wave ($e^{i\omega t}$) traveling in the z direction defined by displacement components

$$u_L = a_L e^{-ik_L z - i\varepsilon_z} e^{i\omega t} = U_L e^{i\omega t},\ u_x = a_x e^{-ik_T z - i\varepsilon_x} e^{i\omega t} = U_x e^{i\omega t},\ u_y = a_y e^{-ik_T z - i\varepsilon_y} e^{i\omega t} = U_y e^{i\omega t}, \quad (12)$$

where k_L and k_T are the longitudinal and transverse wave numbers, ε_L, ε_x, ε_y are the respective phases of the waves, and U_L, U_x, U_y define the complex displacement amplitudes. The intensity in the z direction is

$$I = \frac{\rho\omega^3}{2}\left[\frac{1}{k_T}|U_x|^2 + \frac{1}{k_T}|U_y|^2 + \frac{1}{k_L}|U_L|^2\right]. \quad (13)$$

From the definitions of the electromagnetic Stokes parameters[23] in terms of ensemble averages of plane wave intensities we gain some insight into the choice of the elastic Stokes parameters. For a beam propagating in the z direction they are defined as

$$I_L = \left\langle \frac{\rho\omega^3}{2k_L}|U_L|^2 \right\rangle = \left\langle \frac{\rho\omega^3}{2k_L}a_L^2 \right\rangle,\quad I_x = \left\langle \frac{\rho\omega^3}{2k_T}|U_x|^2 \right\rangle = \left\langle \frac{\rho\omega^3}{2k_T}a_x^2 \right\rangle,\quad I_y = \left\langle \frac{\rho\omega^3}{2k_T}|U_y|^2 \right\rangle = \left\langle \frac{\rho\omega^3}{2k_T}a_y^2 \right\rangle,$$
$$U = \left\langle \frac{\rho\omega^3}{2k_T}2Re(U_x U_y^*) \right\rangle = \left\langle \frac{\rho\omega^3}{k_T}a_x a_y \cos\delta \right\rangle,\qquad V = \left\langle \frac{\rho\omega^3}{2k_T}2Im(U_x U_y^*) \right\rangle = \left\langle \frac{\rho\omega^3}{k_T}a_x a_y \sin\delta \right\rangle. \quad (14)$$

where $\delta = \varepsilon_y - \varepsilon_x$, and the brackets $\langle\rangle$ denote an ensemble average. The first three elastic Stokes parameters have an obvious interpretation. U and V, have less, but are related to coherent interference between the two orthogonally polarized but randomly phased shear waves. U and V may be manifested in an experiment measuring the shear intensity associated with a polarization in a direction other than the x and y directions. The interested reader is directed to the

electromagnetic literature[21,22,23].

The absence of interference terms between the longitudinal and transverse waves is worth noting. The difference in the two wave speeds destroys coherent interference between these two modes after short distances of propagation. A phase relation between shear waves of different polarizations but traveling at the same speed is, however, retained over large distances.

For later convenience a Stokes vector, containing five components, is defined as

$$\underline{I} = \begin{Bmatrix} I_L \\ I_x \\ I_y \\ U \\ V \end{Bmatrix} = \left\langle \frac{\rho\omega^3}{2} \begin{Bmatrix} \frac{|U_L|^2}{k_L} \\ \frac{|U_x|^2}{k_T} \\ \frac{|U_y|^2}{k_T} \\ \frac{2Re(U_x U_y^*)}{k_T} \\ \frac{2Im(U_x U_y^*)}{k_T} \end{Bmatrix} \right\rangle. \tag{15}$$

The average intensity of any beam of diffuse radiation may be fully characterized by its Stokes parameters. It is important to note, though, that for a given propagation direction (here $\hat{\mathbf{z}}$), there is a degree of arbitrariness in the choice of the $\hat{\mathbf{x}}$ direction used for the resolution of polarization. There is, however, a transformation which allows one to calculate the Stokes parameters for one choice of resolution direction in terms of the Stokes parameters for another.

Consider a set of material displacements, u, defined in the xyz coordinate system as shown in Figure 3 with the z direction into the page. From these the Stokes vector, $\underline{I}_1$ can be constructed.

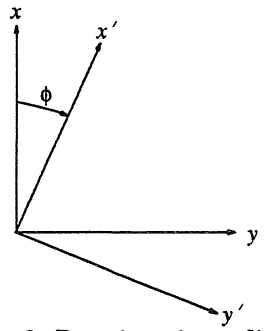

Figure 3. Rotation of coordinates.

These same displacements can be resolved into the $x'y'z$ coordinates where the $x'y'$ axes are oriented an angle ϕ rotated clockwise from the xy axes when viewing in the z direction. In these new coordinates, a new Stokes vector, $\underline{I}_2$, can also be constructed. It can be shown that $\underline{I}_1$ and $\underline{I}_2$ are related through the linear transformation

$$\underline{I}_2 = \underline{\underline{L}}(\phi)\underline{I}_1, \tag{16}$$

where the rotation matrix, $\underline{\underline{L}}(\phi)$, is (see Ishimaru[21], for the electromagnetic case)

$$\underline{\underline{L}}(\phi) = \begin{bmatrix} 1 & 0 & 0 & 0 & 0 \\ 0 & \cos^2\phi & \sin^2\phi & \frac{1}{2}\sin 2\phi & 0 \\ 0 & \sin^2\phi & \cos^2\phi & -\frac{1}{2}\sin 2\phi & 0 \\ 0 & -\sin 2\phi & \sin 2\phi & \cos 2\phi & 0 \\ 0 & 0 & 0 & 0 & 1 \end{bmatrix}. \tag{17}$$

This rotation matrix allows one to see the rotational invariance of the longitudinal component as well as that of the V component which is related to the degree of circular polarization of the transverse waves.

C. Ultrasonic Radiative Transfer Equation

The vector radiative transfer equation for electromagnetic waves is derived using the principal of addition of Stokes parameters. Since the individual Stokes parameters were found to

propagate independently, one can essentially write a transfer equation for each Stokes parameter while accounting for the polarization and scattering effects within the emission term. This has been done in a number of texts[21,23] for the electromagnetic case. Derivation of the ultrasonic radiative transfer equation (URTE) is done in an analogous fashion.

Let us begin as before by writing an energy balance within a small volume *dads*, with $\eta dads$ scatterers. Since the longitudinal and transverse waves propagate without interference we can write separate equations for their respective Stokes parameters. The longitudinal part is governed by the scalar equation

$$\nabla \cdot \hat{\mathbf{p}} I_L(\mathbf{r},t,\hat{\mathbf{p}}) + \frac{1}{c_L}\frac{\partial I_L(\mathbf{r},t,\hat{\mathbf{p}})}{\partial t} + \eta(\kappa_L + \upsilon_L) I_L(\mathbf{r},t,\hat{\mathbf{p}}) = \eta \varepsilon_L(\mathbf{r},t,\hat{\mathbf{p}}), \tag{18}$$

where I_L is the longitudinal Stokes parameter propagating in the $\hat{\mathbf{p}}$ direction, κ_L is the longitudinal scattering coefficient, υ_L the longitudinal absorption coefficient, and ε_L is the longitudinal emission coefficient which includes transverse-to-longitudinal mode conversion effects as well as the non-mode conversion scattering. True internal sources are neglected here but could easily be included.

A transverse vector RTE can also be written using the transverse elastic Stokes parameters I_x, I_y, U, and V. This equation is

$$\nabla \cdot \hat{\mathbf{p}} \underline{I}_T(\mathbf{r},t,\hat{\mathbf{p}},\hat{\mathbf{q}}) + \frac{1}{c_T}\frac{\partial \underline{I}_T(\mathbf{r},t,\hat{\mathbf{p}},\hat{\mathbf{q}})}{\partial t} + \eta(\kappa_T + \upsilon_T)\underline{I}_T(\mathbf{r},t,\hat{\mathbf{p}},\hat{\mathbf{q}}) = \eta \underline{\varepsilon}_T(\mathbf{r},t,\hat{\mathbf{p}},\hat{\mathbf{q}}), \tag{19}$$

where $\underline{I}_T$ is the four component transverse portion of the Stokes vector propagating in the $\hat{\mathbf{p}}$ direction, κ_T and υ_T are the transverse scattering and absorption coefficients, respectively, $\underline{\varepsilon}_T$ is the transverse emission vector which includes all mode conversions into the transverse Stokes

parameters, and $\hat{\mathbf{q}}$ is the direction chosen for the resolution of polarization (perpendicular to $\hat{\mathbf{p}}$.) In general the scattering coefficient is a scattering matrix[29]. However, if the scatterers are spherical or oriented with statistical isotropy the scattering matrix reduces to a scalar coefficient.

Eqs. (18) and (19), one scalar and one vector, are combined into a single Stokes vector equation

$$\nabla \cdot \hat{\mathbf{p}}\underline{I}(\mathbf{r},t,\hat{\mathbf{p}},\hat{\mathbf{q}}) + \underline{\underline{c}}^{-1}\frac{\partial \underline{I}(\mathbf{r},t,\hat{\mathbf{p}},\hat{\mathbf{q}})}{\partial t} + \eta(\underline{\underline{\kappa}}+\underline{\underline{\upsilon}})\underline{I}(\mathbf{r},t,\hat{\mathbf{p}},\hat{\mathbf{q}}) = \eta\underline{\varepsilon}(\mathbf{r},t,\hat{\mathbf{p}},\hat{\mathbf{q}}), \tag{20}$$

where $\underline{I}$ is the Stokes vector from Eq. (15) and

$$\underline{\underline{c}} = \begin{bmatrix} c_L & 0 & 0 & 0 & 0 \\ 0 & c_T & 0 & 0 & 0 \\ 0 & 0 & c_T & 0 & 0 \\ 0 & 0 & 0 & c_T & 0 \\ 0 & 0 & 0 & 0 & c_T \end{bmatrix}, \quad \underline{\underline{\kappa}} = \begin{bmatrix} \kappa_L & 0 & 0 & 0 & 0 \\ 0 & \kappa_T & 0 & 0 & 0 \\ 0 & 0 & \kappa_T & 0 & 0 \\ 0 & 0 & 0 & \kappa_T & 0 \\ 0 & 0 & 0 & 0 & \kappa_T \end{bmatrix}, \quad \underline{\underline{\upsilon}} = \begin{bmatrix} \upsilon_L & 0 & 0 & 0 & 0 \\ 0 & \upsilon_T & 0 & 0 & 0 \\ 0 & 0 & \upsilon_T & 0 & 0 \\ 0 & 0 & 0 & \upsilon_T & 0 \\ 0 & 0 & 0 & 0 & \upsilon_T \end{bmatrix}, \tag{21}$$

and $\underline{\varepsilon}$ is the emission vector for both wave types. As in the scalar case, we define

$$\underline{\underline{P}}(\hat{\mathbf{p}},\hat{\mathbf{q}};\hat{\mathbf{p}}',\hat{\mathbf{q}}')\frac{d\Omega}{4\pi} \tag{22}$$

as the angular distribution of radiation in the $\hat{\mathbf{p}}'$ direction with polarization defined relative to the $\hat{\mathbf{q}}'$ direction scattering into the $\hat{\mathbf{p}}$ direction with polarization defined relative to direction $\hat{\mathbf{q}}$. The emission vector is

$$\underline{\varepsilon}(\mathbf{r},t,\hat{\mathbf{p}},\hat{\mathbf{q}}) = \frac{1}{4\pi}\int_{4\pi}\underline{\underline{P}}(\hat{\mathbf{p}},\hat{\mathbf{q}};\hat{\mathbf{p}}',\hat{\mathbf{q}}')\underline{I}(\mathbf{r},t,\hat{\mathbf{p}}',\hat{\mathbf{q}}')d^2\hat{\mathbf{p}}', \tag{23}$$

and the full ultrasonic radiative transfer equation is then

$$\nabla \cdot \hat{\mathbf{p}}\underline{I}(\mathbf{r},t,\hat{\mathbf{p}},\hat{\mathbf{q}}) + \underline{\underline{c}}^{-1}\frac{\partial \underline{I}(\mathbf{r},t,\hat{\mathbf{p}},\hat{\mathbf{q}})}{\partial t} + \eta(\underline{\underline{\kappa}} + \underline{\underline{\upsilon}})\underline{I}(\mathbf{r},t,\hat{\mathbf{p}},\hat{\mathbf{q}}) = \frac{\eta}{4\pi}\int_{4\pi}\underline{\underline{P}}(\hat{\mathbf{p}},\hat{\mathbf{q}};\hat{\mathbf{p}}',\hat{\mathbf{q}}')\underline{I}(\mathbf{r},t,\hat{\mathbf{p}}',\hat{\mathbf{q}}')d^2\hat{\mathbf{p}}'. \tag{24}$$

After invoking a convention, to be described below, for global resolution of polarization, we may rewrite Eq. (24) in a form without the explicit dependencies on $\hat{\mathbf{q}}$

$$\nabla \cdot \hat{\mathbf{p}}\underline{I}(\mathbf{r},t,\hat{\mathbf{p}}) + \underline{\underline{c}}^{-1}\frac{\partial \underline{I}(\mathbf{r},t,\hat{\mathbf{p}})}{\partial t} + \eta(\underline{\underline{\kappa}} + \underline{\underline{\upsilon}})\underline{I}(\mathbf{r},t,\hat{\mathbf{p}}) = \frac{\eta}{4\pi}\int_{4\pi}\underline{\underline{P}}(\hat{\mathbf{p}},\hat{\mathbf{p}}')\underline{I}(\mathbf{r},t,\hat{\mathbf{p}}')d^2\hat{\mathbf{p}}'. \tag{25}$$

The Mueller or scattering matrix, $\underline{\underline{P}}$, occurring within the integral is determined by examining the scattering from a single particle. This is the subject of subsections D and E.

D. Scattering by a Single Particle

Both the scalar scattering indicatrix, p, and the Mueller matrix, $\underline{\underline{P}}$, are related to the scattering by a single particle. This problem is discussed at great length by a number of authors for electromagnetic waves[23,26,30] and elastic waves[31,32]. The single scattering of a general vector plane wave is depicted in Figure 4. The z and Z directions, being the propagation directions of incident and scattered waves respectively, define the plane of scattering with the longitudinal displacements U_{zi} and U_{Zs} along each of these axes, respectively. The displacements U_{xi} and U_{xs} are perpendicular to this plane while U_{yi} and U_{Ys} both lie in the plane. The scattered Stokes vector is a linear combination of the incident Stokes vector with a $1/r^2$ dependence[33]. This transformation is written[23]

$$\underline{I}_s(\mathbf{r},t,\hat{\mathbf{Z}},\hat{\mathbf{x}}) = \frac{1}{r^2}\underline{\underline{F}}(\hat{\mathbf{Z}},\hat{\mathbf{x}};\hat{\mathbf{z}},\hat{\mathbf{x}})\underline{I}_i(\mathbf{r},t,\hat{\mathbf{z}},\hat{\mathbf{x}}) \tag{26}$$

where the third variable of $\underline{I}$ is the propagation direction and the fourth variable is the direction, $\hat{\mathbf{x}}$, chosen for the resolution of polarization. It is the same for the incident and scattered waves. If the particle has a plane of symmetry normal to the z axis then $\underline{\underline{F}}$ depends only on $\cos\Theta$. $\underline{\underline{F}}$ describes the scattering of the Stokes parameters. A derivation of $\underline{\underline{F}}$ based upon existing descriptions for the scattering of field quantities from spheres is presented in section II.

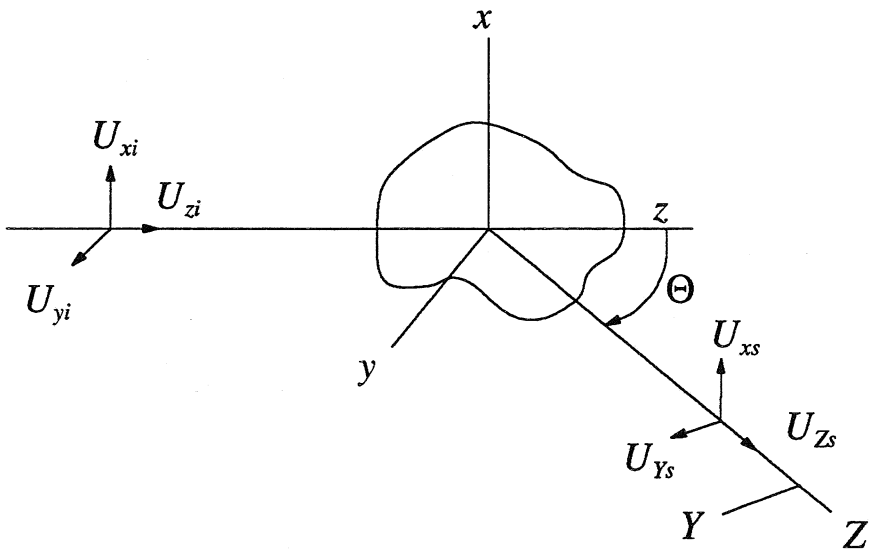

Figure 4. Geometry for single scattering in the local coordinate system.

E. Mueller Matrix

The Mueller matrix, $\underline{\underline{P}}$, in the URTE describes scattering in a global coordinate system. The scattering matrix,$\underline{\underline{F}}$, describing scattering from a single particle, is defined relative to a local coordinate system. An abstract derivation of the relation between $\underline{\underline{F}}$ and $\underline{\underline{P}}$ is given by Ishimaru[23] for a general coordinate system. Since we will use a rectilinear coordinate system, the derivation of $\underline{\underline{P}}$ for electromagnetic waves given by Chandrasekhar[21] and Sekera[34] is followed for derivation of the Mueller matrix for elastic waves in terms of $\underline{\underline{F}}$.

Consider the scattering process defined in an *xyz* rectilinear coordinate system with the scatterer located at the origin as shown in Figure 5. The incident intensity propagates in the $\hat{\mathbf{n}}'$ direction defined by $\mu' = \cos\theta'$ and ϕ' while the scattered intensity is in the $\hat{\mathbf{n}}$ direction defined by $\mu = \cos\theta$ and ϕ. The $\hat{\mathbf{n}}$ and $\hat{\mathbf{n}}'$ directions separated by an angle Θ define the plane of scattering shown shaded in Figure 5.

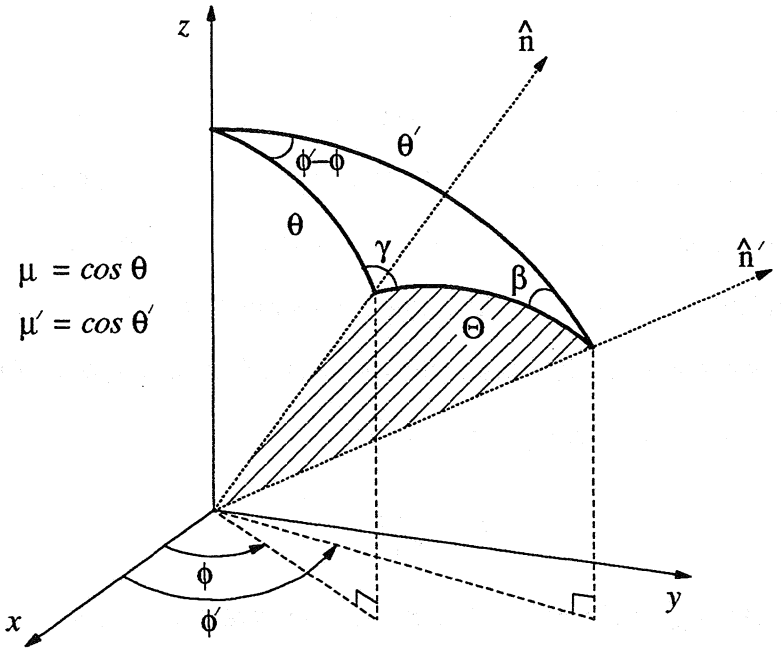

Figure 5. Geometry for scattering in the global coordinate system.

Due to the arbitrary nature of the direction chosen for the resolution of polarization, a reference must be chosen. Let I_{SV} define the intensity in the transverse mode polarized in the direction of increasing θ. I_{SH} then defines the intensity in the transverse mode polarized in the direction of increasing ϕ. With this choice of polarizations I_{SV} is the shear-vertical intensity and I_{SH} is the shear-horizontal intensity[35]. The variables I_x and I_y are reserved for defining the transverse Stokes parameters referred to the local coordinate system characterized by $\underline{\underline{F}}$.

The single scattering matrix, $\underline{\underline{F}}$, was defined with the incident and scattered x and y polarizations perpendicular and parallel, respectively, to the plane of scattering. More complex scattering scenarios with incident and scattered intensities of arbitrary polarization need to be considered. From the single scattering development we know that

$$\underline{I}_s^{ps} = \frac{1}{r^2}\underline{\underline{F}}(\cos\Theta)\underline{I}_i^{ps} \tag{27}$$

where the *ps* superscripts imply that both the incident and scattered Stokes vectors are defined with respect to the plane of scattering. So both $\underline{I}_i^{ps}$ and $\underline{I}_s^{ps}$ have their x polarization components perpendicular to the plane of scattering while their y polarization components are in the plane of scattering. An incident Stokes vector with reference polarization (μ', ϕ') must be rotated an angle of $\beta + \pi/2$ (clockwise when looking in the direction of propagation) to align the incident intensities with the plane of scattering. In other words

$$\underline{I}_i^{ps} = \underline{\underline{L}}\left(\beta + \frac{\pi}{2}\right)\underline{I}_i \tag{28}$$

using the rotation matrix given in Eq. (17). Similarly the scattered Stokes vector with reference polarization (μ, ϕ) is related to the plane of scattering Stokes vector through the rotation

$$\underline{I}_s = \underline{\underline{L}}\left(\gamma - \frac{3\pi}{2}\right)\underline{I}_s^{ps}, \tag{29}$$

so that

$$\underline{\underline{P}}(\mu, \phi; \mu', \phi') = \underline{\underline{L}}\left(\gamma - \frac{3\pi}{2}\right)\underline{\underline{F}}(\cos\Theta)\underline{\underline{L}}\left(\beta + \frac{\pi}{2}\right). \tag{30}$$

By examining the spherical triangle with corners defined by $\hat{\mathbf{n}}$, $\hat{\mathbf{n}}'$, and the z axis, one can determine γ and β in terms of μ, μ', ϕ, and ϕ' so that $\underline{\underline{P}}$ is given in terms of the reference polarization. The dependence of $\underline{\underline{P}}$ on ϕ and ϕ' is seen when this is done. From spherical trigonometry we see that

$$\cos\beta = \frac{1}{\sqrt{1-\chi^2}}[\mu\sqrt{1-\mu'^2} - \mu'\sqrt{1-\mu^2}\cos(\phi'-\phi)],$$

$$\sin\beta = \sqrt{\frac{1-\mu^2}{1-\chi^2}}\sin(\phi'-\phi), \tag{31}$$

$$\cos\gamma = \frac{1}{\sqrt{1-\chi^2}}[\mu'\sqrt{1-\mu^2} - \mu\sqrt{1-\mu'^2}\cos(\phi'-\phi)],$$

$$\sin\gamma = \sqrt{\frac{1-\mu'^2}{1-\chi^2}}\sin(\phi'-\phi),$$

where $\chi = \cos\Theta$. Since $\cos\Theta = \mu\mu' + \sqrt{1-\mu^2}\sqrt{1-\mu'^2}\cos\phi'-\phi$, then $\underline{\underline{F}}$ is even in $\phi'-\phi$. The components of the rotation matrices depend only on combinations of $\cos\beta$, $\sin\beta$, $\cos\gamma$, and $\sin\gamma$ and thus only on $\phi'-\phi$. These facts tell us that $\underline{\underline{P}}$ is also a function only of the combination $\phi'-\phi$. One also finds that the upper left *3x3* and lower right *2x2* of $\underline{\underline{P}}$ are even in $\phi'-\phi$ while the rest of $\underline{\underline{P}}$ is odd in $\phi'-\phi$. So any particle that is described by an $\underline{\underline{F}}$ that depends only on $\cos\Theta$ has a Mueller matrix of this form. These results will be useful when computations are considered.

F. Integrated Intensity and Conservation of Energy

The scattering cross sections must be in some sense integrals of the angular scattering distribution, $\underline{\underline{P}}$, over all outgoing angles. This relation is derived using conservation of energy. We define the integrated intensity, $\underline{i}$, as the integral of the Stokes vector over all solid angles and space

$$\underline{i}(t) = \int \int_{4\pi} \underline{I}(\mathbf{r}, t, \hat{\mathbf{s}}) d^2\hat{\mathbf{s}} d^3\mathbf{r}. \tag{32}$$

From this the time-dependent total energy is

$$E(t) = \underline{e}^{\mathrm{T}} \underline{i}(t), \tag{33}$$

where the vector $\underline{e}^{\mathrm{T}}$ is given by

$$\underline{e}^{\mathrm{T}} = \left\{ \frac{1}{c_L}, \frac{1}{c_T}, \frac{1}{c_T}, 0, 0 \right\}, \tag{34}$$

and the superscript **T** signifies a transpose. Eq. (25) is multiplied on the left by $\underline{\underline{c}}$ and then by $\underline{e}^{\mathrm{T}}$ and integrated over all angles, $\hat{\mathbf{p}}$, and space to give

$$\frac{d}{dt}(\underline{e}^{\mathrm{T}} \underline{i}(t)) + \eta \underline{e}^{\mathrm{T}} \underline{\underline{c}} (\underline{\underline{\kappa}} + \underline{\underline{\upsilon}}) \underline{i}(t) = \eta \underline{e}^{\mathrm{T}} \underline{\underline{c}}\, \underline{\underline{\Delta}}\, \underline{i}(t), \tag{35}$$

where use has been made of the divergence theorem. The matrix $\underline{\underline{\Delta}}$ is defined as

$$\underline{\underline{\Delta}} = \frac{1}{4\pi} \int_{4\pi} \underline{\underline{P}}(\hat{\mathbf{p}}, \hat{\mathbf{p}}') d^2\hat{\mathbf{p}}', \tag{36}$$

which is independent of $\hat{\mathbf{p}}$ if the scattering is statistically isotropic. If the absorption matrix, $\underline{\underline{\upsilon}}$, is zero the change in energy with respect to time is zero which implies

$$\underline{e}^{\mathrm{T}} \underline{\underline{c}}\, \underline{\underline{\kappa}}\, \underline{i}(t) = \underline{e}^{\mathrm{T}} \underline{\underline{c}}\, \underline{\underline{\Delta}}\, \underline{i}(t). \tag{37}$$

This must be true for all $\underline{i}$. Recalling the components of $\underline{\underline{\kappa}}$, one concludes

$$\kappa_L = \frac{1}{4\pi}\int_{4\pi} P_{11} + P_{21} + P_{31} d^2\hat{\mathbf{p}}',$$

$$\kappa_T = \frac{1}{4\pi}\int_{4\pi} P_{12} + P_{22} + P_{32} d^2\hat{\mathbf{p}}', \tag{38}$$

$$\kappa_T = \frac{1}{4\pi}\int_{4\pi} P_{13} + P_{23} + P_{33} d^2\hat{\mathbf{p}}'.$$

We find it convenient to calculate κ_T by

$$\kappa_T = \frac{1}{2}\frac{1}{4\pi}\int_{4\pi} P_{12} + P_{13} + P_{22} + P_{23} + P_{32} + P_{33} d^2\hat{\mathbf{p}}'. \tag{39}$$

The ordinary differential equation given in Eq. (35) without $\underline{e}^{\mathrm{T}}$ may also be examined. It is

$$\frac{d\underline{i}(t)}{dt} = \eta(\underline{\underline{\Delta}} - \underline{\underline{\kappa}} - \underline{\underline{\upsilon}})\underline{i}(t). \tag{40}$$

The eigenvalues and eigenvectors of the matrix on the right-hand side of Eq. (40) tell us about the time dependence of the integrated intensity. Without absorption, one would expect to find one solution with zero eigenvalue representing an equipartition amongst the energies in different modes. But four other solutions also exist. These solutions contain information about the scattering between modes of the integrated intensity. Writing out the non-absorptive eigenmatrix gives

$$\begin{bmatrix} \Delta_{11} - \kappa_L & \Delta_{12} & \Delta_{13} & \Delta_{14} & \Delta_{15} \\ \Delta_{21} & \Delta_{22} - \kappa_T & \Delta_{23} & \Delta_{24} & \Delta_{25} \\ \Delta_{31} & \Delta_{32} & \Delta_{33} - \kappa_T & \Delta_{34} & \Delta_{35} \\ \Delta_{41} & \Delta_{42} & \Delta_{43} & \Delta_{44} - \kappa_T & \Delta_{45} \\ \Delta_{51} & \Delta_{52} & \Delta_{53} & \Delta_{54} & \Delta_{55} - \kappa_T \end{bmatrix}. \tag{41}$$

Inserting the values of the κ'*s* from Eq. (38) gives

$$\begin{bmatrix} -\Delta_{21}-\Delta_{31} & \Delta_{12} & \Delta_{13} & \Delta_{14} & \Delta_{15} \\ \Delta_{21} & -\Delta_{12}-\Delta_{32} & \Delta_{23} & \Delta_{24} & \Delta_{25} \\ \Delta_{31} & \Delta_{32} & -\Delta_{13}-\Delta_{23} & \Delta_{34} & \Delta_{35} \\ \Delta_{41} & \Delta_{42} & \Delta_{43} & \Delta_{44}-\Delta_{12}-\Delta_{22}-\Delta_{32} & \Delta_{45} \\ \Delta_{51} & \Delta_{52} & \Delta_{53} & \Delta_{54} & \Delta_{55}-\Delta_{12}-\Delta_{22}-\Delta_{32} \end{bmatrix}. \quad (42)$$

If $\underline{\underline{P}}$ is constructed as described in Eq. (30) and $\underline{\underline{F}}$ depends only on $\cos\Theta$ then some simplification to this eigenmatrix can be attained. In this case the 10 components that are odd in $\phi'-\phi$, namely Δ_{14}, Δ_{15}, Δ_{24}, Δ_{25}, Δ_{34}, Δ_{35}, Δ_{41}, Δ_{42}, Δ_{43}, Δ_{51}, Δ_{52}, and Δ_{53} are all zero leaving the eigenmatrix

$$\begin{bmatrix} -\Delta_{21}-\Delta_{31} & \Delta_{12} & \Delta_{13} & 0 & 0 \\ \Delta_{21} & -\Delta_{12}-\Delta_{32} & \Delta_{23} & 0 & 0 \\ \Delta_{31} & \Delta_{32} & -\Delta_{13}-\Delta_{23} & 0 & 0 \\ 0 & 0 & 0 & \Delta_{44}-\Delta_{12}-\Delta_{22}-\Delta_{32} & \Delta_{45} \\ 0 & 0 & 0 & \Delta_{54} & \Delta_{55}-\Delta_{12}-\Delta_{22}-\Delta_{32} \end{bmatrix}. \quad (43)$$

So the integrated intensity related to the U and V parameters decouples from the others. The upper left *3x3* matrix is further simplified if we assume, again, that the medium is statistically isotropic. In this case

$$\Delta_{12}=\Delta_{13}, \quad \Delta_{21}=\Delta_{31}=(c_L/c_T)^2\Delta_{12}, \quad \Delta_{32}=\Delta_{23}. \quad (44)$$

Solving for the eigensystem gives us the eigenvalues, α, and their eigenvectors, $\underline{\Psi}$,

$$\alpha_1=0, \underline{\Psi}_1=\begin{Bmatrix} 1 \\ (c_L/c_T)^2 \\ (c_L/c_T)^2 \end{Bmatrix}; \quad \alpha_2=-(\Delta_{12}+2\Delta_{23}), \underline{\Psi}_2=\begin{Bmatrix} 0 \\ -1 \\ 1 \end{Bmatrix}; \quad \alpha_3=-\Delta_{12}(1+2(c_L/c_T)^2), \underline{\Psi}_3=\begin{Bmatrix} -2 \\ 1 \\ 1 \end{Bmatrix}. \quad (45)$$

The first eigensolution is the steady-state equipartition as expected. It has an eigenvector corresponding to an equipartitioning of energy[36]. The second eigensolution describes a decay

due to mode conversion between the two transverse modes while the third eigensolution apparently describes the decay in time due to mode conversion between the longitudinal and transverse modes.

G. Nondimensionalization in a Semi-infinite, Plane-parallel Medium

Consider now a medium which extends infinitely in the $+z$ direction and $\pm x$ and $\pm y$ directions and has a boundary at $z=0$ as shown previously for the scalar case in Figure 2 with $z_b \to \infty$. Let the intensity be invariant under translation in the x and y directions. The time dependence is retained for now. Thus the intensity varies only with z, t, $\mu = \cos\theta$, and ϕ as measured from the x axis toward the y axis. The URTE then reduces to

$$\mu \frac{\partial \underline{I}(z,t,\mu,\phi)}{\partial z} + \underline{\underline{c}}^{-1} \frac{\partial \underline{I}(z,t,\mu,\phi)}{\partial t} + \eta(\underline{\underline{\kappa}} + \underline{\underline{\upsilon}})\underline{I}(z,t,\mu,\phi) = \frac{\eta}{4\pi} \int_{-1}^{+1} \int_{0}^{2\pi} \underline{\underline{P}}(\mu,\phi;\mu',\phi')\underline{I}(z,t,\mu',\phi')d\mu' d\phi', \tag{46}$$

The depth dependence is nondimensionalized by defining the *transverse ultrasonic depth* (analogous to optical depth in the classical theory) as

$$\tau = \int_0^z \eta \kappa_T dz. \tag{47}$$

For a homogeneous medium κ_T is constant so that $\tau = \eta \kappa_T z$. Thus the depth is measured in units of inverse shear wave attenuation. For a homogeneous medium a dimensionless time variable is similarly defined as $\xi = \eta c_T \kappa_T t$. Time is now measured in units of the mean time between shear ray scatterings. These dimensionless variables give the nondimensional URTE

$$\mu\frac{\partial \underline{I}(\tau,\xi,\mu,\phi)}{\partial\tau}+\underline{\underline{\tilde{c}}}^{-1}\frac{\partial \underline{I}(\tau,\xi,\mu,\phi)}{\partial\xi}+(\underline{\underline{\tilde{\kappa}}}+\underline{\underline{\tilde{\upsilon}}})\underline{I}(\tau,\xi,\mu,\phi)= \tag{48}$$

$$\frac{1}{4\pi\kappa_T}\int_{-1}^{+1}\int_{0}^{2\pi}\underline{\underline{P}}(\mu,\phi;\mu',\phi')\underline{I}(\tau,\xi,\mu',\phi')d\mu'd\phi',$$

where

$$\underline{\underline{\tilde{c}}}=\frac{1}{c_T}\begin{bmatrix} c_L & 0 & 0 & 0 & 0\\ 0 & c_T & 0 & 0 & 0\\ 0 & 0 & c_T & 0 & 0\\ 0 & 0 & 0 & c_T & 0\\ 0 & 0 & 0 & 0 & c_T \end{bmatrix},\ \underline{\underline{\tilde{\kappa}}}=\frac{1}{\kappa_T}\begin{bmatrix} \kappa_L & 0 & 0 & 0 & 0\\ 0 & \kappa_T & 0 & 0 & 0\\ 0 & 0 & \kappa_T & 0 & 0\\ 0 & 0 & 0 & \kappa_T & 0\\ 0 & 0 & 0 & 0 & \kappa_T \end{bmatrix},\ \underline{\underline{\tilde{\upsilon}}}=\frac{1}{\kappa_T}\begin{bmatrix} \upsilon_L & 0 & 0 & 0 & 0\\ 0 & \upsilon_T & 0 & 0 & 0\\ 0 & 0 & \upsilon_T & 0 & 0\\ 0 & 0 & 0 & \upsilon_T & 0\\ 0 & 0 & 0 & 0 & \upsilon_T \end{bmatrix}. \tag{49}$$

The total extinction coefficient, σ, which is the sum of the scattering and absorption coefficients is now defined for later use. This coefficient also has a nondimensional counterpart, $\tilde{\sigma}$. These new variables are

$$\sigma_{L/T}=\kappa_{L/T}+\upsilon_{L/T},\qquad \tilde{\sigma}_{L/T}=\frac{\sigma_{L/T}}{\kappa_T}, \tag{50}$$

where the *L/T* implies that this relation holds for either mode but the nondimensionalization is done with respect to the transverse scattering coefficient, κ_T. If we now concentrate on the steady-state problem, the time derivative term may be neglected. For a harmonic plane wave incident at the surface the boundary conditions are

$$\underline{I}(\tau=0,\mu>0,\phi)=\underline{I}_0\delta(\mu-\mu_0)\delta(\phi-\phi_0),\qquad \underline{I}(\tau\to\infty,\mu<0,\phi)=0. \tag{51}$$

where $\underline{I}_0$ is the amplitude vector of the incident intensities in the (μ_0, ϕ_0) direction. The second boundary condition is the radiation boundary condition at infinity. Note that the boundary conditions are split in their μ dependence.

The above homogeneous boundary-value problem with nonhomogeneous boundary conditions is turned into a nonhomogeneous BVP with homogeneous boundary conditions by the following method (see Ishimaru[23], for the scalar case and Ishimaru[29], for the electromagnetic vector case). Consider the intensity vector to be composed of two parts - the original pulse attenuated (reduced incident intensity in the radiative transfer literature), $\underline{I}_{r.i.}$ and the diffuse intensity, $\underline{I}_d$ which has been scattered at least once. The reduced incident intensity is

$$\underline{I}_{r.i.} = \left[\begin{Bmatrix} I_{LO} \\ 0 \\ 0 \\ 0 \\ 0 \end{Bmatrix} e^{-\tilde{\sigma}_L \tau/\mu} + \begin{Bmatrix} 0 \\ I_{SVO} \\ I_{SHO} \\ U_0 \\ V_0 \end{Bmatrix} e^{-\tilde{\sigma}_T \tau/\mu} \right] \delta(\mu - \mu_0)\delta(\phi - \phi_0) \tag{52}$$

where the *0* subscript indicates the incident intensity. The incident Stokes vector given by Eq. (52) is just a combination of incident longitudinal and transverse waves in the (μ_0, ϕ_0) direction attenuating through the depth due to both scattering and absorption. Then if $\underline{I} = \underline{I}_{r.i.} + \underline{I}_d$ is substituted into the steady-state version of Eq. (48) we find

$$\mu \frac{\partial \underline{I}_d(\tau, \mu, \phi)}{\partial \tau} + (\underline{\underline{\tilde{\kappa}}} + \underline{\underline{\tilde{\upsilon}}})\underline{I}_d(z, \mu, \phi) = \frac{1}{4\pi} \int_{-1}^{+1} \int_{0}^{2\pi} \underline{\underline{P}}(\mu, \phi; \mu', \phi') \underline{I}_d(\tau, \mu', \phi') d\mu' d\phi' + \underline{S}_L(\mu, \phi; \mu_0, \phi_0) e^{-\tilde{\sigma}_L \tau/\mu_0} + \underline{S}_T(\mu, \phi; \mu_0, \phi_0) e^{-\tilde{\sigma}_T \tau/\mu_0}, \tag{53}$$

to be the equation governing the diffuse intensity, where

$$\underline{S}_L(\mu, \phi; \mu_0, \phi_0) = \frac{1}{4\pi\kappa_T} \underline{\underline{P}}(\mu, \phi; \mu_0, \phi_0) \begin{Bmatrix} I_{LO} \\ 0 \\ 0 \\ 0 \end{Bmatrix}, \quad \underline{S}_T(\mu, \phi; \mu_0, \phi_0) = \frac{1}{4\pi\kappa_T} \underline{\underline{P}}(\mu, \phi; \mu_0, \phi_0) \begin{Bmatrix} 0 \\ I_{SVO} \\ I_{SHO} \\ U_0 \\ V_0 \end{Bmatrix}, \tag{54}$$

represent sources of diffuse intensity. The diffuse intensity has the homogeneous boundary conditions

$$\underline{I}_d(z=0,\mu>0,\phi)=\underline{I}_d(z\to\infty,\mu<0,\phi)=0. \tag{55}$$

The d subscript on the diffuse intensity is now dropped. The two source terms, $\underline{S}_L$ and $\underline{S}_T$, in Eq. (53) represent the incident intensity that has been scattered once, while the integral in Eq. (53) represents all scatterings of two or more. The singly scattered solution is of interest for comparison to the full multiply scattered intensity and is discussed in the next subsection.

H. Singly Scattered Solution

The equation governing the singly scattered intensity is Eq. (53) with the integral term removed:

$$\frac{\partial \underline{I}(\tau,\mu,\phi)}{\partial\tau}+\frac{1}{\mu}(\tilde{\underline{\underline{\kappa}}}+\tilde{\underline{\underline{\upsilon}}})\underline{I}(\tau,\mu,\phi)=\frac{1}{\mu}\underline{S}_L(\mu,\phi;\mu_0,\phi_0)e^{-\tilde{\sigma}_L\tau/\mu_0}+\frac{1}{\mu}\underline{S}_T(\mu,\phi;\mu_0,\phi_0)e^{-\tilde{\sigma}_T\tau/\mu_0}. \tag{56}$$

This vector equation has the same form as the scalar equation

$$\frac{dI(\tau)}{d\tau}+aI(\tau)=g(\tau), \tag{57}$$

where $g(\tau)$ represents the source function. Eq. (57) has a general solution of the form[37]

$$I(\tau)=ce^{-a\tau}+e^{-a\tau}\int^{\tau}e^{a\tau'}g(\tau')d\tau'. \tag{58}$$

with c determined by the boundary conditions. It is convenient to distinguish the upward moving intensity, I^- (for $\mu<0$) from the downward intensity, I^+ (for $\mu>0$). The singly scattered intensity, I^-, in the upward direction at any depth, τ, comes solely from the medium below it. The downward intensity, I^+, comes from the medium above τ. Thus

$$I^- = c^- e^{+|a|\tau} + e^{+|a|\tau} \int_{\tau}^{\infty} e^{-|a|\tau'} g(\tau') d\tau', \qquad \mu < 0$$

$$I^+ = c^+ e^{-|a|\tau} + e^{-|a|\tau} \int_{0}^{\tau} e^{+|a|\tau'} g(\tau') d\tau', \qquad \mu > 0 \tag{59}$$

where c^- and c^+ are determined from the boundary conditions. Because the downward intensity, I^+, is zero at the upper surface and the upward intensity, I^-, is zero at infinity, both of these coefficients vanish.

Eqs. (59) describe the singly scattered field in a scalar RTE. Because, in the URTE, 'a' depends on wave type, it is convenient to decompose the solution into longitudinal and transverse types. Thus, the following definitions are in order. The forcing terms, $\underline{S}_L$ and $\underline{S}_T$, are decomposed into their longitudinal and transverse parts as

$$\underline{S}_L = \begin{Bmatrix} S_{LL} \\ \underline{S}_{LT} \end{Bmatrix}, \qquad \underline{S}_T = \begin{Bmatrix} S_{TL} \\ \underline{S}_{TT} \end{Bmatrix}, \tag{60}$$

where the scalars S_{LL} and S_{TL} are the longitudinal components and the vectors $\underline{S}_{LT}$ and $\underline{S}_{TT}$ are the four transverse components of the forcing terms. The intensity is similarly decomposed as

$$\underline{I} = \begin{Bmatrix} I_L \\ \underline{I}_T \end{Bmatrix}. \tag{61}$$

From Eqs. (59) we write

$$I_L^{\pm}(\tau, \mu, \phi) = \frac{e^{-\tilde{\sigma}_L \tau/\mu}}{|\mu|} \int_{0,\tau}^{\tau,\infty} e^{-\tilde{\sigma}_L \tau'/\mu} \left[S_{LL} e^{-\tilde{\sigma}_L \tau'/\mu_0} + S_{TL} e^{-\tilde{\sigma}_T \tau'/\mu_0} \right] d\tau', \tag{62}$$

where the limits of integration are $(0, \tau)$ for I_L^+ and (τ, ∞) for I_L^-. The integrations are performed giving the singly scattered longitudinal intensity

$$I_L^-(\tau,\mu<0,\phi)=-\frac{1}{\mu}\left[S_{LL}\frac{e^{-\tilde{\sigma}_L\tau/\mu_0}}{(\tilde{\sigma}_L/\mu_0-\tilde{\sigma}_L/\mu)}+S_{TL}\frac{e^{-\tilde{\sigma}_T\tau/\mu_0}}{(\tilde{\sigma}_T/\mu_0-\tilde{\sigma}_L/\mu)}\right],$$
$$I_L^+(\tau,\mu>0,\phi)=\frac{1}{\mu}\left[S_{LL}\frac{e^{-\tilde{\sigma}_L\tau/\mu}-e^{-\tilde{\sigma}_L\tau/\mu_0}}{(\tilde{\sigma}_L/\mu_0-\tilde{\sigma}_L/\mu)}+S_{TL}\frac{e^{-\tilde{\sigma}_L\tau/\mu}-e^{-\tilde{\sigma}_T\tau/\mu_0}}{(\tilde{\sigma}_T/\mu_0-\tilde{\sigma}_L/\mu)}\right]. \quad (63)$$

The transverse part of the singly scattered intensities, $\underline{I}_T$, is similarly

$$\underline{I}_T^-(\tau,\mu<0,\phi)=-\frac{1}{\mu}\left[\underline{S}_{LT}\frac{e^{-\tilde{\sigma}_L\tau/\mu_0}}{(\tilde{\sigma}_L/\mu_0-\tilde{\sigma}_T/\mu)}+\underline{S}_{TT}\frac{e^{-\tilde{\sigma}_T\tau/\mu_0}}{(\tilde{\sigma}_T/\mu_0-\tilde{\sigma}_T/\mu)}\right],$$
$$\underline{I}_T^+(\tau,\mu>0,\phi)=\frac{1}{\mu}\left[\underline{S}_{LT}\frac{e^{-\tilde{\sigma}_T\tau/\mu}-e^{-\tilde{\sigma}_L\tau/\mu_0}}{(\tilde{\sigma}_L/\mu_0-\tilde{\sigma}_T/\mu)}+\underline{S}_{TT}\frac{e^{-\tilde{\sigma}_T\tau/\mu}-e^{-\tilde{\sigma}_T\tau/\mu_0}}{(\tilde{\sigma}_T/\mu_0-\tilde{\sigma}_T/\mu)}\right]. \quad (64)$$

The total singly scattered intensity is the superposition of the longitudinal and transverse components and is a function of the Mueller matrix and the scattering and absorption coefficients. Comparison of the singly scattered solution with the full solution provides a measure of the amount of multiple scattering occurring. One could formally write out other terms defining the double scatter, triple scatter, etc., but only the singly scattered intensity can be expressed in simple closed form for a general $\underline{\underline{P}}$.

II. SCATTERING BY A SPHERICAL OBSTACLE IN AN ISOTROPIC SOLID

In order to solve the URTE, the Mueller matrix, $\underline{\underline{P}}$, must be specified in accordance with the scattering nature of the medium. This section is devoted to deriving the Mueller matrix for spherical obstacles contained in an isotropic solid. The derivation of $\underline{\underline{F}}$ is first presented in terms of Legendre polynomial expansions representing the scattered displacements. Then the Mueller matrix is constructed from $\underline{\underline{F}}$ using Eq. (30) with the two rotation matrices.

An exact solution for the scattered displacements of a linearly polarized electromagnetic wave incident on a spherical scatterer was found by Mie[30] in 1908. The Mie theory has since been used by many authors[23,26,33] to define the scattering from a sphere in terms of the Stokes parameters. A similar solution for an arbitrary elastic wave incident on a sphere can be found by decomposing the incident wave into a longitudinal wave and a transverse wave, each scattering separately. The scattered Stokes vector can be found for each case and the two solutions superposed to give the general case. Mathematically this decomposition is expressed as

$$\underline{I}_s = \frac{1}{r^2}\underline{\underline{F}}\,\underline{I}_i = \frac{1}{r^2}[\underline{\underline{F}}_L\underline{I}_{Li} + \underline{\underline{F}}_T\underline{I}_{Ti}] = \frac{1}{r^2}\left[\underline{\underline{F}}_L\begin{Bmatrix} I_{Li} \\ 0 \\ 0 \\ 0 \end{Bmatrix} + \underline{\underline{F}}_T\begin{Bmatrix} 0 \\ I_{xi} \\ I_{yi} \\ U_i \\ V_i \end{Bmatrix}\right], \tag{65}$$

where $\underline{\underline{F}}_L$ and $\underline{\underline{F}}_T$ are the scattering matrices due to incident longitudinal and transverse waves, respectively, and I_{Li}, I_{xi}, I_{yi}, U_i and V_i are the incident Stokes parameters defined in the local coordinate system. Since the elastic Stokes parameters depend on the complex displacement amplitudes, one needs to calculate the scattered displacement fields given an incident displacement field. The longitudinal scattering matrix is found with help from Ying and Truell[31] and the transverse scattering matrix is found using Einspruch, Witterholt, and Truell[32].

A. Scattering of an Incident Longitudinal Wave

The scattering of an elastic longitudinal wave from a spherical scatterer was solved by Ying and Truell[31] (YT) to find the scattering cross-section defined as the ratio of the scattered energy to the incident energy. Their work is now recast into a radiative transfer form involving Stokes parameters for substitution into the URTE. They considered a unit displacement amplitude incident plane longitudinal wave propagating in the z direction and impinging on a

sphere located at the origin as shown in Figure 6. The scattered field's

$$u_s = \nabla\psi_s + \nabla \times (\hat{\phi}\partial\Pi_s/\partial\Theta), \tag{66}$$

displacement potentials were expanded as

$$\begin{aligned} \psi_s &= \sum_{m=0}^{\infty} A_m h_m(k_L r) P_m(\cos\Theta), \\ \Pi_s &= \sum_{m=0}^{\infty} B_m h_m(k_T r) P_m(\cos\Theta). \end{aligned} \tag{67}$$

where $k_L = \omega/c_L$ and $k_T = \omega/c_T$ are the longitudinal and transverse wavenumbers, respectively, h_m the mth order, spherical Hankel function, and P_m is the mth degree Legendre polynomial, with the angle Θ defined as the angle between the incident wave's propagation direction and that of the observation position in the direction of the scattered wave. The A_m's and B_m's have units of length and are found by considering the appropriate boundary conditions at the surface of the sphere at $r=a$. Ying and Truell calculated these coefficients for an isotropically elastic sphere, a spherical cavity, and a rigid sphere; they are treated here as known quantities.

Our goal is to find the scattered elastic Stokes parameters in terms of the incident Stokes parameters. Using the potentials given by Eq. (67), and approximating the Hankel function[26] for $kr \gg 1$ we calculate the scattered displacements

$$\begin{aligned} s_{rs} &= \frac{1}{r} e^{ik_L r} \sum_{m=0}^{\infty} A_m (-i)^m P_m(\cos\Theta) = \frac{1}{r} e^{ik_L r} f_L(\chi), \\ s_{\Theta s} &= \frac{1}{r} e^{ik_T r} \sum_{m=1}^{\infty} B_m (-i)^m P_m^1(\cos\Theta) = \frac{1}{r} e^{ik_T r} f_{Ly}(\chi), \end{aligned} \tag{68}$$

where $\chi = \cos\Theta$ and Eq. (68) serves to define the functions $f(\chi)$ in terms of the field scattering coefficients A and B. Note that $s_{\phi s}$ is zero because of the symmetry of both the scatterer and the

incident wave. Inasmuch as we have assumed $kr \gg 1$, we have limited the applicability of the results of this section to cases in which successive scattering events are separated by distances large compared to $1/k$. Similar restrictions, in the form $\alpha/k \ll 1$, have been noted elsewhere[18].

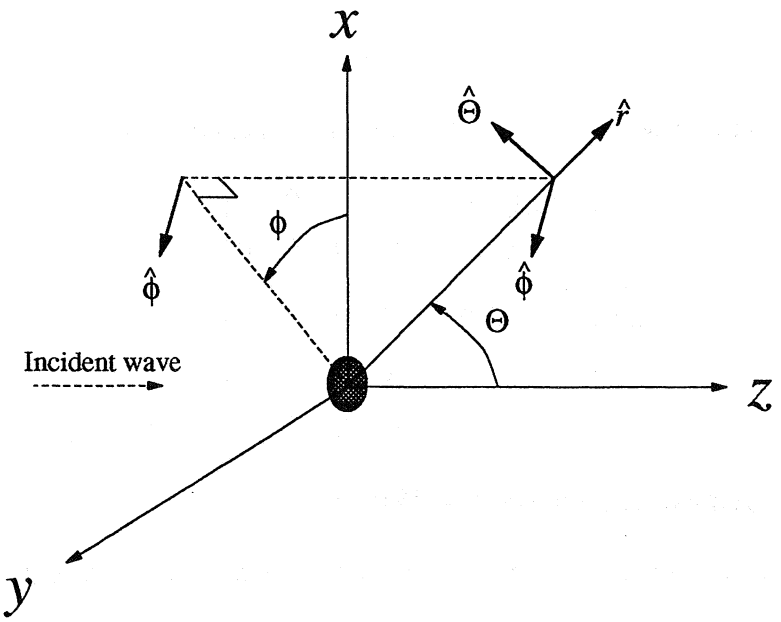

Figure 6. Geometry for the scattering of an incident longitudinal or transverse wave from a spherical scatterer. The scattered waves are defined in the $\hat{r}$, $\hat{\Theta}$, and $\hat{\phi}$ directions.

Using the definitions of the elastic Stokes parameters in Eq. (14) we find that the scattered Stokes parameters are

$$I_L = \frac{\rho\omega^3}{2k_L}|s_{rs}|^2 = \frac{\rho\omega^3}{2k_L r^2}|f_L(\chi)|^2, \qquad I_y = \frac{\rho\omega^3}{2k_T}|s_{\Theta s}|^2 = \frac{\rho\omega^3}{2k_T r^2}|f_{Ly}(\chi)|^2. \tag{69}$$

Thus the scattered Stokes vector is

$$\underline{I}_{Ls} = \frac{\rho\omega^3}{2k_L r^2}\begin{Bmatrix} |f_L(\chi)|^2 \\ 0 \\ \frac{k_L}{k_T}|f_{Ly}(\chi)|^2 \\ 0 \\ 0 \end{Bmatrix}. \tag{70}$$

The incident Stokes vector for a unit amplitude longitudinal wave is

$$\underline{I}_{Li} = \frac{\rho\omega^3}{2k_L}\begin{Bmatrix}1\\0\\0\\0\\0\end{Bmatrix}. \tag{71}$$

The longitudinal portion of the scattering matrix from Eq. (65) is therefore

$$\underline{\underline{F}}_L = \begin{bmatrix} |f_L(\chi)|^2 & 0 & 0 & 0 & 0 \\ 0 & 0 & 0 & 0 & 0 \\ \frac{k_L}{k_T}|f_{Ly}(\chi)|^2 & 0 & 0 & 0 & 0 \\ 0 & 0 & 0 & 0 & 0 \\ 0 & 0 & 0 & 0 & 0 \end{bmatrix}. \tag{72}$$

B. Scattering of an Incident Transverse Wave

Einspruch, Witterholt, and Truell[32] (EWT) calculated the scattering cross-section for a unit amplitude plane transverse wave, polarized in the x direction, incident on a sphere. The scattering geometry is shown in Figure 6. Because of the polarization of the incident shear wave there is no longer azimuthal symmetry and the three displacement components of the vector Helmholtz equation do not decouple. Following Morse and Feshbach[38] they obtain scattered displacements of the form

$$s_{rs} = \sum_{m=1}^{\infty} \cos\phi P_m^1[b_m A_1(r) + d_m A_2(r)],$$

$$s_{\Theta s} = \sum_{m=1}^{\infty} \frac{\cos\phi}{\sqrt{1-\chi^2}}\left\{a_m P_m^1 B_1(r) + \left[\frac{m}{m+1}P_{m+1}^1 - \frac{m+1}{m}P_{m-1}^1\right][b_m B_2(r) + d_m B_3(r)]\right\}, \tag{73}$$

$$s_{\phi s} = \sum_{m=1}^{\infty} \frac{\sin\phi}{\sqrt{1-\chi^2}}\left\{a_m\left[\frac{m}{m+1}P_{m+1}^1 - \frac{m+1}{m}P_{m-1}^1\right]D_1(r) + P_m^1[b_m D_2(r) + d_m D_3(r)]\right\},$$

where P_m^1 is the first order *mth* degree Legendre polynomial of $\chi = \cos\Theta$, and a_m, b_m, and d_m are coefficients found from considering boundary conditions at the surface of the sphere $r=a$. These coefficients are dimensionless and are given explicitly by (EWT) for a rigid sphere, a spherical cavity, an elastic sphere, and a fluid-filled cavity and will be considered knowns throughout this work. The functions A, B, and D are given by (EWT) in terms of spherical Hankel functions and are not repeated here.

Again we approximate the Hankel function for $kr \gg 1$ to obtain the far-field displacements

$$
\begin{aligned}
s_{rs} &= \cos\phi \frac{1}{r} e^{ik_L r} \sum_{m=1}^{\infty} \frac{1}{k_L} d_m P_m^1 \frac{(2m+1)}{m(m+1)} = \cos\phi \frac{1}{r} e^{ik_L r} f_{yL}(\chi), \\
s_{\Theta s} &= \cos\phi \frac{1}{r} e^{ik_T r} \sum_{m=1}^{\infty} \frac{i}{k_T \sin\Theta} \left\{ a_m P_m^1 \frac{(2m+1)}{m(m+1)} + b_m \left[\frac{m}{m+1} P_{m+1}^1 - \frac{m+1}{m} P_{m-1}^1 \right] \right\}, \\
&= \cos\phi \frac{1}{r} e^{ik_T r} f_y(\chi), \qquad (74) \\
s_{\phi s} &= \sin\phi \frac{1}{r} e^{ik_T r} \sum_{m=1}^{\infty} \frac{i}{k_T \sin\Theta} \left\{ a_m \left[\frac{m}{m+1} P_{m+1}^1 - \frac{m+1}{m} P_{m-1}^1 \right] + b_m P_m^1 \frac{(2m+1)}{m(m+1)} \right\}, \\
&= \sin\phi \frac{1}{r} e^{ik_T r} f_x(\chi).
\end{aligned}
$$

where Eqs. (74) define the f functions. It should be noted that $f_x(\chi)$ and $f_y(\chi)$ have the same angular dependencies as S_1 and S_2 given by van de Hulst[28] for Mie scattering. This is expected due the transverse nature of both elastic shear waves and electromagnetic waves.

The case considered by (EWT) is not the most general case for incident shear waves. To fully formulate the transverse scattering matrix for the ultrasonic radiative transfer equation we need to consider two orthogonally polarized, out-of-phase shear waves incident on the scatterer

from the same direction. This more complex case is calculated from the single wave case by superposition. First consider an incoming shear wave polarized in the x direction with amplitude a_x. This is essentially the case considered by (EWT) so the scattered displacements are

$$s_{rsx} = a_x \cos\phi \frac{1}{r} e^{ik_L r} f_{yL}(\chi), \quad s_{\Theta sx} = a_x \cos\phi \frac{1}{r} e^{ik_T r} f_y(\chi), \quad s_{\phi sx} = a_x \sin\phi \frac{1}{r} e^{ik_T r} f_x(\chi). \tag{75}$$

We can also examine an incoming shear wave polarized in the y direction with amplitude a_y and a phase lag δ with respect to the x-polarized wave. The scattered displacements are shifted by the same phase and are given by

$$s_{rsy} = a_y \sin\phi \frac{1}{r} e^{ik_L r - i\delta} f_{yL}(\chi), \quad s_{\Theta sy} = a_y \sin\phi \frac{1}{r} e^{ik_T r - i\delta} f_y(\chi), \quad s_{\phi sy} = -a_y \cos\phi \frac{1}{r} e^{ik_T r - i\delta} f_x(\chi). \tag{76}$$

The two sets of displacements given in Eqs. (75) and (76) are now added giving the total displacement field due to the incoming waves

$$\begin{aligned} s_{rs} &= s_{rsx} + s_{rsy} = \frac{1}{r} e^{ik_L r} f_{yL}(\chi) [a_x \cos\phi + a_y \sin\phi e^{-i\delta}], \\ s_{\Theta s} &= s_{\Theta sx} + s_{\Theta sy} = \frac{1}{r} e^{ik_T r} f_y(\chi) [a_x \cos\phi + a_y \sin\phi e^{-i\delta}], \\ s_{\phi s} &= s_{\phi sx} + s_{\phi sy} = \frac{1}{r} e^{ik_T r} f_x(\chi) [a_x \sin\phi - a_y \cos\phi e^{-i\delta}]. \end{aligned} \tag{77}$$

The scattered Stokes parameters are constructed from the definitions in Eq. (14)

$$\begin{aligned} I_{Ls} &= \frac{\rho\omega^3}{2k_L} |s_{rs}|^2 = \frac{\rho\omega^3}{2k_L r^2} |f_{yL}(\chi)|^2 [a_x^2 \cos^2\phi + a_y^2 \sin^2\phi + a_x a_y \sin 2\phi \cos\delta], \\ I_{xs} &= \frac{\rho\omega^3}{2k_T} |-s_{\phi s}|^2 = \frac{\rho\omega^3}{2k_T r^2} |f_x(\chi)|^2 [a_x^2 \sin^2\phi + a_y^2 \cos^2\phi - a_x a_y \sin 2\phi \cos\delta], \\ I_{ys} &= \frac{\rho\omega^3}{2k_T} |s_{\Theta s}|^2 = \frac{\rho\omega^3}{2k_T r^2} |f_y(\chi)|^2 [a_x^2 \cos^2\phi + a_y^2 \sin^2\phi + a_x a_y \sin 2\phi \cos\delta], \end{aligned} \tag{78}$$

$$U_s = \frac{\rho\omega^3}{k_T} Re(-s_{\phi s} s_{\Theta s}^*),$$

$$= \frac{\rho\omega^3}{2k_T r^2} \{Re(f_x f_y^*)[a_x^2 \sin 2\phi - a_y^2 \sin 2\phi - 2a_x a_y \cos\delta \cos 2\phi] - Im(f_x f_y^*)[2a_x a_y \sin\delta]\},$$

$$V_s = \frac{\rho\omega^3}{2k_T} 2Im(-s_{\phi s} s_{\Theta s}^*),$$

$$= \frac{\rho\omega^3}{2k_T r^2} \{Im(f_x f_y^*)[a_x^2 \sin 2\phi - a_y^2 \sin 2\phi - 2a_x a_y \cos\delta \cos 2\phi] + Re(f_x f_y^*)[2a_x a_y \sin\delta]\}.$$

The incident Stokes vector, $\underline{I}'_i$, in the coordinate system used by (EWT) is

$$\underline{I}'_i = \frac{\rho\omega^3}{2k_T} \begin{Bmatrix} 0 \\ a_x^2 \\ a_y^2 \\ 2a_x a_y \cos\delta \\ 2a_x a_y \sin\delta \end{Bmatrix}. \tag{79}$$

The transverse scattering matrix, $\underline{\underline{F}}_T$, was defined with both incident and scattered x polarizations perpendicular to the plane of scattering and the y polarizations in the plane of scattering. However, the incident Stokes vector, $\underline{I}_i'$, given in Eq. (79) does not have the appropriate polarization as the scattered Stokes parameters given in Eqs. (78). Therefore the Stokes vector, $\underline{I}'_i$, given in Eq. (79) must be rotated an angle ϕ clockwise when viewed in the direction of increasing z. Thus, $\underline{I}_i = \underline{\underline{L}}(\phi)\underline{I}'_i$, or

$$\underline{I}_i = \frac{\rho\omega^3}{2k_T}\begin{bmatrix} 1 & 0 & 0 & 0 & 0 \\ 0 & \cos^2\phi & \sin^2\phi & \frac{1}{2}\sin 2\phi & 0 \\ 0 & \sin^2\phi & \cos^2\phi & -\frac{1}{2}\sin 2\phi & 0 \\ 0 & -\sin 2\phi & \sin 2\phi & \cos 2\phi & 0 \\ 0 & 0 & 0 & 0 & 1 \end{bmatrix} \begin{Bmatrix} 0 \\ a_x^2 \\ a_y^2 \\ 2a_x a_y \cos\delta \\ 2a_x a_y \sin\delta \end{Bmatrix}. \tag{80}$$

This gives the incident Stokes vector with I_x perpendicular and I_y parallel to the plane of scattering as

$$\underline{I}_i = \frac{\rho\omega^3}{2k_T}\begin{Bmatrix} 0 \\ a_x^2\sin^2\phi + a_y^2\cos^2\phi - a_x a_y \sin 2\phi\cos\delta \\ a_x^2\cos^2\phi + a_y^2\sin^2\phi + a_x a_y \sin 2\phi\cos\delta \\ a_x^2\sin 2\phi - a_y^2\sin 2\phi - 2a_x a_y \cos 2\phi\cos\delta \\ 2a_x a_y \sin\delta \end{Bmatrix}. \tag{81}$$

Finally, the decomposition in Eq. (65) gives us the transverse scattering matrix

$$\underline{\underline{F}}_T = \begin{bmatrix} 0 & 0 & \frac{k_T}{k_L}|f_{yL}(\chi)|^2 & 0 & 0 \\ 0 & |f_x(\chi)|^2 & 0 & 0 & 0 \\ 0 & 0 & |f_y(\chi)|^2 & 0 & 0 \\ 0 & 0 & 0 & Re(f_x f_y^*) & -Im(f_x f_y^*) \\ 0 & 0 & 0 & Im(f_x f_y^*) & Re(f_x f_y^*) \end{bmatrix}. \tag{82}$$

C. Total Scattering Matrix

The solutions from the two cases considered above are now superposed to give the general solution of elastic wave scattering from a sphere. For any incident Stokes vector, $\underline{I}_i$, the scattered Stokes vector, $\underline{I}_s$, is be given by Eq. (65) where $\underline{\underline{F}}$ is given by the sum of $\underline{\underline{F}}_L$ and $\underline{\underline{F}}_T$

$$\underline{\underline{F}}(\chi)=\begin{bmatrix} |f_L(\chi)|^2 & 0 & \frac{k_T}{k_L}|f_{yL}(\chi)|^2 & 0 & 0 \\ 0 & |f_x(\chi)|^2 & 0 & 0 & 0 \\ \frac{k_L}{k_T}|f_{Ly}(\chi)|^2 & 0 & |f_y(\chi)|^2 & 0 & 0 \\ 0 & 0 & 0 & Re(f_x f_y^*) & -Im(f_x f_y^*) \\ 0 & 0 & 0 & Im(f_x f_y^*) & Re(f_x f_y^*) \end{bmatrix} \tag{83}$$

where the scattering functions are given by the following expansions:

$$f_L(\chi)=\sum_{m=0}^{\infty} A_m(-i)^m P_m,$$

$$f_{Ly}(\chi)=\sum_{m=1}^{\infty} B_m(-i)^m P_m^1,$$

$$f_{yL}(\chi)=\sum_{m=1}^{\infty}\frac{1}{k_L}d_m P_m^1\frac{(2m+1)}{m(m+1)}, \tag{84}$$

$$f_x(\chi)=\sum_{m=1}^{\infty}\frac{i}{k_T\sin\Theta}\left\{b_m P_m^1\frac{(2m+1)}{m(m+1)}+a_m\left[\frac{m}{m+1}P_{m+1}^1-\frac{m+1}{m}P_{m-1}^1\right]\right\},$$

$$f_y(\chi)=\sum_{m=1}^{\infty}\frac{i}{k_T\sin\Theta}\left\{a_m P_m^1\frac{(2m+1)}{m(m+1)}+b_m\left[\frac{m}{m+1}P_{m+1}^1-\frac{m+1}{m}P_{m-1}^1\right]\right\}.$$

The scattering matrix has the form expected due to the symmetry of the scatterer[23].

D. Mueller Matrix for a Spherical Scatterer

The relationship between $\underline{\underline{P}}$ and $\underline{\underline{F}}$ was given in Eq. (30) where it was stated that γ and β could be put in terms of μ, μ', ϕ, and ϕ' by examining the spherical triangle (Fig. 5) defined by the incident and scattered intensities and the z axis. Doing this and defining the four variables *(r,d), (l,d), (d,r),* and *(d,l),* we find

$$\cos\beta=\frac{(r,d)}{\sqrt{1-\chi^2}}=\frac{1}{\sqrt{1-\chi^2}}[\mu\sqrt{1-\mu'^2}-\mu'\sqrt{1-\mu^2}\cos(\phi'-\phi)],$$

$$\sin\beta=\frac{(l,d)}{\sqrt{1-\chi^2}}=\sqrt{\frac{1-\mu^2}{1-\chi^2}}\sin(\phi'-\phi),$$

$$\cos\gamma=\frac{(d,r)}{\sqrt{1-\chi^2}}=\frac{1}{\sqrt{1-\chi^2}}[\mu'\sqrt{1-\mu^2}-\mu\sqrt{1-\mu'^2}\cos(\phi'-\phi)], \tag{85}$$

$$\sin\gamma=\frac{-(d,l)}{\sqrt{1-\chi^2}}=\sqrt{\frac{1-\mu'^2}{1-\chi^2}}\sin(\phi'-\phi).$$

Using these definitions in the rotation matrices and $\underline{\underline{F}}$ given in Eq. (83) for a spherical scatterer, the Mueller matrix for a spherical scatterer is

$$\underline{\underline{P}}(\mu,\phi,\mu',\phi')=\begin{bmatrix} |f_{11}|^2 & \frac{k_T}{k_L}|f_{12}|^2 & \frac{k_T}{k_L}|f_{13}|^2 & \frac{k_T}{k_L}Re(f_{12}f_{13}^*) & 0 \\ \frac{k_L}{k_T}|f_{21}|^2 & |f_{22}|^2 & |f_{23}|^2 & Re(f_{22}f_{23}^*) & -Im(f_{22}f_{23}^*) \\ \frac{k_L}{k_T}|f_{31}|^2 & |f_{32}|^2 & |f_{33}|^2 & Re(f_{32}f_{33}^*) & -Im(f_{32}f_{33}^*) \\ 2\frac{k_L}{k_T}Re(f_{21}f_{31}^*) & 2Re(f_{22}f_{32}^*) & 2Re(f_{23}f_{33}^*) & Re(f_{22}f_{33}^*+f_{23}f_{32}^*) & -Im(f_{22}f_{33}^*-f_{23}f_{32}^*) \\ 0 & 2Im(f_{22}f_{32}^*) & 2Im(f_{23}f_{33}^*) & Im(f_{22}f_{33}^*+f_{23}f_{32}^*) & Re(f_{22}f_{33}^*-f_{23}f_{32}^*) \end{bmatrix} \tag{86}$$

where, using the functions defined in Eq. (85) and some additional notation introduced by Chandrasekhar[21] and Sekera[34], we have

$$f_{11}=f_L,\quad f_{12}=(r,d)f_{yL},\quad f_{13}=(l,d)f_{yL}\quad f_{21}=(d,r)f_{Ly},\quad f_{31}=(d,l)f_{Ly}$$

$$f_{22}=(l,l)T_1+(r,r)T_2,\qquad f_{23}=-(r,l)T_1+(l,r)T_2$$

$$f_{32}=-(l,r)T_1+(r,l)T_2,\qquad f_{33}=(r,r)T_1+(l,l)T_2$$

$$T_1=\frac{f_x-\chi f_y}{1-\chi^2},\qquad T_2=\frac{f_y-\chi f_x}{1-\chi^2}$$

$$(l,l)=\sqrt{1-\mu^2}\sqrt{1-\mu'^2}+\mu\mu'\cos(\phi'-\phi),\qquad (r,r)=\cos(\phi'-\phi)$$
$$(l,r)=-\mu'\sin(\phi'-\phi),\qquad (r,l)=\mu\sin(\phi'-\phi) \tag{87}$$

$$f_L(\chi)=\sum_{m=0}^{\infty}A_m(-i)^m P_m^0(\chi),\qquad f_{Ly}(\chi)=\sum_{m=1}^{\infty}\frac{(-i)^m}{\sqrt{1-\chi^2}}B_m P_m^1(\chi),\qquad f_{yL}(\chi)=\sum_{m=1}^{\infty}\frac{d_m}{k_L\sqrt{1-\chi^2}}\frac{(2m+1)}{m(m+1)}P_m^1(\chi)$$

$$f_x(\chi)=\sum_{m=1}^{\infty}\frac{i}{k_T\sqrt{1-\chi^2}}\left\{b_m P_m^1(\chi)\frac{(2m+1)}{m(m+1)}+a_m\left[\frac{m}{m+1}P_{m+1}^1(\chi)-\frac{m+1}{m}P_{m-1}^1(\chi)\right]\right\},$$

$$f_y(\chi)=\sum_{m=1}^{\infty}\frac{i}{k_T\sqrt{1-\chi^2}}\left\{a_m P_m^1(\chi)\frac{(2m+1)}{m(m+1)}+b_m\left[\frac{m}{m+1}P_{m+1}^1(\chi)-\frac{m+1}{m}P_{m-1}^1(\chi)\right]\right\},$$

$$\mu=\cos\theta,\qquad \mu'=\cos\theta',\qquad \chi=\cos\Theta=\mu\mu'+\sqrt{1-\mu^2}\sqrt{1-\mu'^2}\cos(\phi'-\phi).$$

The definitions of f_{Ly} and f_{yL} have been changed slightly to include all the χ dependence. If the longitudinal portion (row 1 and column 1) is neglected, $\underline{\underline{P}}$ is identical in form to that given by Ishimaru[29] based on the Mie solution. The symmetry properties discussed by Hovenier[39] and van de Hulst[26] also hold for the elastic Mueller matrix with the added complication of mode conversion. The dependence on $\phi'-\phi$ discussed previously is explicitly seen as is the fact that the upper left *3x3* and lower right *2x2* sub-matrices of $\underline{\underline{P}}$ are even in $\phi'-\phi$ while all other terms are odd in $\phi'-\phi$.

From the conservation of energy relation given in Eqs. (38) and (39) the scattering coefficients for spherical scatterers are

$$\kappa_L=\kappa_{LL}+\kappa_{LT}=\frac{1}{4\pi}\int_{4\pi}P_{11}d^2\hat{\mathbf{p}}'+\frac{1}{4\pi}\int_{4\pi}P_{21}+P_{31}d^2\hat{\mathbf{p}}',$$

$$\kappa_L=\sum_{m=0}^{\infty}\frac{1}{2m+1}\left[|A_m|^2+m(m+1)\frac{k_L}{k_T}|B_m|^2\right], \tag{88}$$

$$\kappa_T = \kappa_{TL} + \kappa_{TT} = \frac{1}{8\pi}\int_{4\pi} P_{12} + P_{13} d^2\hat{\mathbf{p}}' + \frac{1}{8\pi}\int_{4\pi} P_{22} + P_{23} + P_{32} + P_{33} d^2\hat{\mathbf{p}}'$$

$$\kappa_T = \sum_{m=0}^{\infty} \frac{2m+1}{2}\left[\frac{1}{k_T^2}|a_m|^2 + \frac{1}{k_T^2}|b_m|^2 + \frac{k_T}{k_L^3 m(m+1)}|d_m|^2\right].$$

The κ'*s* defined in Eqs. (88) are equal to the single scattering cross-sections for spheres given by (YT) and (EWT) divided by 4π, as expected.

III. SOLUTION OF THE URTE

For the scalar plane-parallel RTE a number of solution techniques exist, some analytical and some numerical. For an isotropic scatterer and for a Rayleigh scatterer Chandrasekhar reduced this problem to finding the solution to simple nonlinear integral equations. However, for the more complex vector radiative transfer equations which include polarization effects no analytical tools exist for a general Mueller matrix. Instead we must examine numerical approaches. In this paper we consider the simple case of a semi-infinite homogeneous medium with the intensity invariant under *x* and *y* translations. The time dependent problem will be discussed briefly but the time dependent case will not be solved. Any specifications to the form of the Mueller matrix will be made when needed. Within this context the nonhomogeneous URTE is

$$\mu\frac{\partial \underline{I}(\tau,\xi,\mu,\phi)}{\partial\tau} + \underline{\underline{\tilde{c}}}^{-1}\frac{\partial \underline{I}(\tau,\xi,\mu,\phi)}{\partial\xi} + (\underline{\underline{\tilde{\kappa}}} + \underline{\underline{\tilde{\upsilon}}})\underline{I}(\tau,\xi,\mu,\phi) =$$
$$\frac{1}{4\pi}\int_{-1}^{+1}\int_{0}^{2\pi} \underline{\underline{P}}(\mu,\phi;\mu',\phi')\underline{I}(\tau,\xi,\mu',\phi')d\mu' d\phi' + \underline{S}_L(\mu,\phi;\mu_0,\phi,\xi)e^{-\tilde{\sigma}_L\tau/\mu_0} + \underline{S}_T(\mu,\phi;\mu_0,\phi_0,\xi)e^{-\tilde{\sigma}_T\tau/\mu_0}, \tag{89}$$

with boundary conditions

$$\underline{I}(z=0,\mu>0,\phi)=0, \quad \underline{I}(z\to\infty,\mu<0,\phi)=0. \tag{90}$$

The boundary reflection, although very important for elastic wave problems, is neglected in this paper in order to minimize the complications.

A. Temporal Fourier Transform

The time derivative is removed by defining the Fourier transform pair

$$\tilde{\underline{I}}(\tau,\Omega,\mu,\phi)=\int_{-\infty}^{+\infty}\underline{I}(\tau,\xi,\mu,\phi)e^{-i\Omega\xi}d\xi,$$
$$\underline{I}(\tau,\xi,\mu,\phi)=\frac{1}{2\pi}\int_{-\infty}^{+\infty}\tilde{\underline{I}}(\tau,\Omega,\mu,\phi)e^{i\Omega\xi}d\Omega. \tag{91}$$

The transformed URTE then becomes

$$\mu\frac{\partial\tilde{\underline{I}}(\tau,\Omega,\mu,\phi)}{\partial\tau}+\left(\tilde{\underline{\underline{\kappa}}}+\tilde{\underline{\underline{\upsilon}}}+i\Omega\tilde{\underline{\underline{c}}}^{-1}\right)\tilde{\underline{I}}(\tau,\Omega,\mu,\phi)=$$
$$\frac{1}{4\pi\kappa_T}\int_{-1}^{+1}\int_{0}^{2\pi}\underline{\underline{P}}(\mu,\phi;\mu',\phi')\tilde{\underline{I}}(\tau,\Omega,\mu',\phi')d\mu'd\phi'+\tilde{\underline{S}}_L(\mu,\phi;\mu_0,\phi,\Omega)e^{-\tilde{\sigma}_L\tau/\mu_0}+\tilde{\underline{S}}_T(\mu,\phi;\mu_0,\phi_0,\Omega)e^{-\tilde{\sigma}_T\tau/\mu_0}. \tag{92}$$

Since we will be considering the steady-state case, Ω is set to zero at this time and the tilde above $\underline{I}$, $\underline{S}_L$, $\underline{S}_T$ dropped. If the time domain solution were needed, the transformed URTE could be solved in frequency space as outlined below for each Ω and the solution then transformed back to the time domain.

B. Azimuthal Fourier Decomposition

For the Mueller matrix constructed for spherical scatterers it is easy to see that $\underline{\underline{P}}$ depends on ϕ and ϕ' only by means of the combination $\phi'-\phi$ as mentioned above. This dependence lends itself to a Fourier expansion in $\phi'-\phi$ and decoupling of the Fourier components. This procedure

is also valid whenever $\underline{\underline{P}}$ can be constructed using the rotation matrices and $\underline{\underline{F}}$ is only a function of $\cos\Theta$. This property is expected for all statistically axisymmetric media. We first expand the Mueller matrix in a finite number of Fourier terms

$$\underline{\underline{P}}(\mu,\mu',\phi'-\phi)=\sum_{m=-M}^{+M}\underline{\underline{P}}_m(\mu,\mu')e^{-im(\phi'-\phi)}, \tag{93}$$

so that

$$\underline{\underline{P}}_m(\mu,\mu')=\frac{1}{2\pi}\int_0^{2\pi}\underline{\underline{P}}(\mu,\mu',\phi'-\phi)e^{+im(\phi'-\phi)}d(\phi'-\phi). \tag{94}$$

The Stokes vector is also expanded

$$\underline{I}(\tau,\mu,\phi)=\sum_{l=-L}^{+L}\underline{I}_l(\tau,\mu)e^{il(\phi'-\phi_0)}, \tag{95}$$

where ϕ_0 may be set to zero without loss of generality.

Substitution into the transformed URTE gives for each $m=-M...+M$,

$$\mu\frac{\partial\underline{I}_m(\tau,\mu)}{\partial\tau}+(\underline{\underline{\tilde{\kappa}}}+\underline{\underline{\tilde{\upsilon}}})\underline{I}_m(\tau,\mu)= \frac{1}{2\kappa_T}\int_{-1}^{+1}\underline{\underline{P}}_m(\mu,\mu')\underline{I}_m(\tau,\mu')d\mu'+\underline{S}_{Lm}(\mu,\mu_0)e^{-\tilde{\sigma}_L\tau/\mu_0}+\underline{S}_{Tm}(\mu,\mu_0)e^{-\tilde{\sigma}_T\tau/\mu_0}, \tag{96}$$

where the orthogonality of the Fourier series terms has been used and

$$\underline{S}_{Lm}(\mu,\mu_0)=\frac{1}{4\pi\kappa_T}\underline{\underline{P}}_m(\mu,\mu_0)\begin{Bmatrix}I_{L0}\\0\\0\\0\\0\end{Bmatrix},\qquad \underline{S}_{Tm}(\mu,\mu_0)=\frac{1}{4\pi\kappa_T}\underline{\underline{P}}_m(\mu,\mu_0)\begin{Bmatrix}0\\I_{SV0}\\I_{SH0}\\U_0\\V_0\end{Bmatrix}. \tag{97}$$

We are still left with an integro-differential equation that cannot be solved analytically for a general Mueller matrix. Therefore a numerical method is used for its solution.

C. Discrete Ordinates Method

A variety of numerical techniques are available for solving this set of equations including the easily implemented discrete ordinates method[21,23]. In essence, the Stokes vector, $\underline{I}_m$, is discretized in the direction coordinate μ and the integral is approximated using Gaussian quadrature[21,23,27]. A different quadrature rule could also be used and there has been much debate over which is more accurate[27]. Using Gaussian quadrature we find the discretized URTE for the *mth* Fourier component and *ith* direction, μ_i, as

$$\mu_i \frac{\partial \underline{I}^i_m(\tau)}{\partial \tau} + \underline{\underline{\tilde{\sigma}}}\,\underline{I}^i_m(\tau) - \frac{1}{2\kappa_T} \sum_{\substack{j=-N \\ j\neq 0}}^{+N} a_j \underline{\underline{P}}^{ij}_m \underline{I}^j_m(\tau) = \underline{S}^i_{Lm} e^{-\tilde{\sigma}_L \tau/\mu_0} + \underline{S}^i_{Tm} e^{-\tilde{\sigma}_T \tau/\mu_0}, \tag{98}$$

where

$$\underline{I}^i_m(\tau) = \underline{I}_m(\tau, \mu_i), \quad \underline{\underline{P}}^{ij}_m = \underline{\underline{P}}_m(\mu_i, \mu_j), \quad \underline{S}^i_{(L/T)m} = \underline{S}_{(L/T)m}(\mu_i, \mu_0), \tag{99}$$

and $\underline{\underline{\tilde{\sigma}}} = \underline{\underline{\tilde{\kappa}}} + \underline{\underline{\tilde{\upsilon}}}$ and the a_j'*s* and μ_j'*s* are the weights and divisions, respectively, of the Gaussian quadrature. The boundary conditions are now

$$\underline{I}^i_m(\tau = 0) = 0, \quad i > 0; \qquad \underline{I}^i_m(\tau \to \infty) = 0, \quad i < 0. \tag{100}$$

This discretization is put in a form more suited for computations by defining a new vector, **I**, containing the Stokes vectors for each of the directional components

$$\mathbf{I}_m(\tau) = \begin{Bmatrix} \underline{I}^{-N}_m(\tau) \\ \cdot \\ \cdot \\ \cdot \\ \underline{I}^{+N}_m(\tau) \end{Bmatrix}, \tag{101}$$

which allows Eq. (98) to be written

$$\frac{d\mathbf{I}_m(\tau)}{d\tau} + \mathbf{W}_m \mathbf{I}_m(\tau) = \mathbf{S}_{Lm} e^{-\tilde{\sigma}_L \tau/\mu_0} + \mathbf{S}_{Tm} e^{-\tilde{\sigma}_T \tau/\mu_0}, \tag{102}$$

where

$$\mathbf{W}_m = \begin{bmatrix} \frac{\tilde{\sigma}}{\mu_{-N}} & & \\ & \ddots & \\ & & \frac{\tilde{\sigma}}{\mu_{+N}} \end{bmatrix} - \frac{1}{2\kappa_T} \begin{bmatrix} \frac{a_{-N}}{\mu_{-N}} \underline{\underline{P}}^{-N,-N}_m & \cdots & \frac{a_{+N}}{\mu_{-N}} \underline{\underline{P}}^{-N,+N}_m \\ \vdots & \cdots & \vdots \\ \frac{a_{-N}}{\mu_{+N}} \underline{\underline{P}}^{+N,-N}_m & \cdots & \frac{a_{+N}}{\mu_{+N}} \underline{\underline{P}}^{+N,+N}_m \end{bmatrix}, \tag{103}$$

and

$$\mathbf{S}_{Lm} = \begin{Bmatrix} \frac{\underline{S}^{-N}_{Lm}}{\mu_{-N}} \\ \vdots \\ \frac{\underline{S}^{+N}_{Lm}}{\mu_{+N}} \end{Bmatrix}, \quad \mathbf{S}_{Tm} = \begin{Bmatrix} \frac{\underline{S}^{-N}_{Tm}}{\mu_{-N}} \\ \vdots \\ \frac{\underline{S}^{+N}_{Tm}}{\mu_{+N}} \end{Bmatrix}. \tag{104}$$

Since we have discretized the intensity in $2N$ directions, $\mathbf{W}_m$ is a $10N$x$10N$ matrix and $\mathbf{I}_m$, $\mathbf{S}_{Lm}$, and $\mathbf{S}_{Tm}$ are $10N$x1 column vectors. Note that the upper half (i<0) of $\mathbf{I}_m$, $\mathbf{S}_{Lm}$, and $\mathbf{S}_{Tm}$ is the upward propagating intensity while the lower half (i>0) is the downward propagating intensity. The original integro-differential URTE given in Eq. (89) has now been reduced to an ODE with the homogeneous boundary conditions

$$\mathbf{I}^+_m(\tau = 0) = 0, \qquad \mathbf{I}^-_m(\tau \to \infty) = 0, \tag{105}$$

where $\mathbf{I}^+_m$ is the lower half of $\mathbf{I}_m$ and $\mathbf{I}^-_m$ is the upper half of $\mathbf{I}_m$.

The solution of Eq. (102) consists of a particular solution, $\mathbf{I}_m^P$, for the two source terms, and a homogeneous solution, $\mathbf{I}_m^H$. The particular solution is given by

$$\mathbf{I}_m^P(\tau) = \mathbf{H}_m^L e^{-\tilde{\sigma}_L \tau/\mu_0} + \mathbf{H}_m^T e^{-\tilde{\sigma}_T \tau/\mu_0}, \tag{106}$$

where

$$\mathbf{H}_m^L = \left[\mathbf{W}_m - \mathbf{D}\frac{\tilde{\sigma}_L}{\mu_0}\right]^{-1} \mathbf{S}_{Lm}, \quad \mathbf{H}_m^T = \left[\mathbf{W}_m - \mathbf{D}\frac{\tilde{\sigma}_T}{\mu_0}\right]^{-1} \mathbf{S}_{Tm}, \tag{107}$$

with **D** defining the *10Nx10N* identity matrix.

The homogeneous part of the discretized intensity, $\mathbf{I}_m^H(\tau)$, is a solution to the equation

$$\frac{d\mathbf{I}_m^H(\tau)}{d\tau} + \mathbf{W}_m \mathbf{I}_m^H(\tau) = 0. \tag{108}$$

Looking for solutions of the form

$$\mathbf{I}_m^H(\tau) = \mathbf{g}_m e^{-\lambda_m \tau}, \tag{109}$$

we obtain an eigenvalue problem for the *mth* Fourier component

$$\mathbf{W}_m \mathbf{g}_m = \lambda_m \mathbf{g}_m. \tag{110}$$

Once the *10N* distinct eigensolutions, λ_{mn} and $\mathbf{g}_{mn}$ (n = *1,2,3, . . . 10N*) of $\mathbf{W}_m$ are found, the homogeneous solution is written as a linear combination of them

$$\mathbf{I}_m^H(\tau) = \sum_{n=0}^{10N} C_{mn} \mathbf{g}_{mn} e^{-\lambda_{mn} \tau}, \tag{111}$$

and the full solution is

$$\mathbf{I}_m(\tau) = \sum_{n=0}^{10N} C_{mn} \mathbf{g}_{mn} e^{-\lambda_{mn} \tau} + \mathbf{H}_m^L e^{-\tilde{\sigma}_L \tau/\mu_0} + \mathbf{H}_m^T e^{-\tilde{\sigma}_T \tau/\mu_0}. \tag{112}$$

where the coefficients C_{mn} are determined from the boundary conditions given in Eq. (105). For the semi-infinite medium considered here there is no upward radiation incident at $\tau = \infty$. From this radiation boundary condition one concludes that

$$C_{mn} = 0 \quad \forall \quad \lambda_{mn} < 0 \tag{113}$$

For the rest of the C_{mn}'s we must separate the upward and downward propagating intensities. At the surface $\tau = 0$ we find

$$\mathbf{I}_m(0) = \begin{Bmatrix} \mathbf{I}_m^- \\ \mathbf{I}_m^+ \end{Bmatrix} = \sum_{n=0}^{5N} C_{mn} \begin{Bmatrix} \mathbf{g}_{mn}^- \\ \mathbf{g}_{mn}^+ \end{Bmatrix} + \begin{Bmatrix} \mathbf{H}_m^{L-} \\ \mathbf{H}_m^{L+} \end{Bmatrix} + \begin{Bmatrix} \mathbf{H}_m^{T-} \\ \mathbf{H}_m^{T+} \end{Bmatrix}. \tag{114}$$

The remaining boundary condition implies that

$$\sum_{n=0}^{5N} C_{mn} \mathbf{g}_{mn}^+ + \mathbf{H}_m^{L+} + \mathbf{H}_m^{T+} = 0, \tag{115}$$

or

$$\begin{aligned} \mathbf{G}_m \mathbf{C}_m &= -[\mathbf{H}_m^{L+} + \mathbf{H}_m^{T+}], \\ \mathbf{C}_m &= -\mathbf{G}_m^{-1}[\mathbf{H}_m^{L+} + \mathbf{H}_m^{T+}], \end{aligned} \tag{116}$$

where Eqs. (115) and (116) define the matrix $\mathbf{G}_m$ and vector $\mathbf{C}_m$. The eigenvalue problem given in Eq. (110) has some interesting properties due to the symmetries of $\mathbf{W}_m$ as discussed by Ishimaru[23] for the scalar case. For instance, all eigenvalues will occur in $\pm$ pairs and without absorption one of these pairs will be identically zero corresponding to the diffusion limit.

IV. RESULTS

The above equations for the discretized, steady-state, *x-y* independent URTE were solved for the case of randomly distributed spherical voids. Results for two different normally incident waves are presented. Both of these problems are axisymmetric. Results for a normally incident

longitudinal wave are presented first followed by results for two incoherent, orthogonally polarized shear waves at normal incidence. The medium is assumed to have a wavespeed ratio of $c_L/c_T = 2$. The absorption rate per wavelength for the two modes is set equal

$$c_L \upsilon_L = c_T \upsilon_T. \tag{117}$$

The intensity components are examined as functions of angle, depth into the medium, and absorption. Results will be presented in terms of the nondimensional transverse absorption (absorption rate per scattering rate), $\tilde{\upsilon}_T = \upsilon_T/\kappa_T$. Frequency dependent absorption was not considered here but would be necessary for any comparison to real materials. High absorption corresponds to early times where single scattering dominates and multiple scattering effects are largely unimportant. For this reason, singly scattered results will be used for comparison in some cases. The equations were solved on a SUN Sparcstation using various IMSL subroutines (Eigen solver, linear equation solver, etc.). The number of terms used in the expansions (Eqs. (87)) of the scattering functions was frequency dependent, being increased until convergence was attained.

To show that the model describes the full multiple scattering range the approach to the diffusion limit deep within the medium also is presented. In this limit the field becomes very nearly isotropic and, due to equipartitioning of energy, the relationship between the intensity components should be[36]

$$I_{SV} = I_{SH} = \left(\frac{c_L}{c_T}\right)^2 I_L. \tag{118}$$

A. Longitudinal Wave Normally Incident

A longitudinal wave at normal incidence ($\mu_0 = 1$) corresponds to an axisymmetric disturbance, thus only one Fourier series term is needed (m=0). In this case the U and V components decouple due to the $\phi' - \phi$ dependence of $\underline{\underline{P}}$ mentioned earlier. The transverse forcing term $\underline{S}_{T0}$ is zero and the longitudinal one is (assuming unit intensity of the incident wave)

$$\underline{S}_{L0} = \frac{1}{2\kappa_T} \begin{Bmatrix} P_{11,0}(\mu, \mu_0 = 1) \\ P_{21,0}(\mu, \mu_0 = 1) \\ P_{31,0}(\mu, \mu_0 = 1) \\ 0 \\ 0 \end{Bmatrix}. \tag{119}$$

where

$$P_{ij,0}(\mu, \mu') = \frac{1}{2\pi} \int_0^{2\pi} P_{ij}(\mu, \mu', \phi' - \phi) d(\phi' - \phi), \tag{120}$$

is the zeroeth order Fourier expansion of the *ijth* component of $\underline{\underline{P}}$.

For an incident longitudinal wave, the L-L scattering plays a primary role. The angular dependence of P_{11} governs this scattering. A polar plot of P_{11} is shown in Figure 7 for two frequencies ($k_L a$ = 0.05, 1.5) with the incident wave impinging on the spherical void from the left. The backward and forward scattering tendencies are obvious. The actual amplitude of the low frequency graph (Fig. 7a) is 10^8 times smaller than the amplitude for the high frequency graph (Fig. 7b) corresponding to the much smaller scattering cross section for long wavelength scattering.

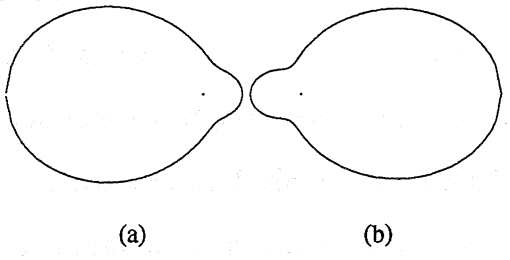

Figure 7. Polar plot of P_{11} (a: $k_L a = 0.05$, b: $k_L a = 1.5$). The actual amplitude for (a) is 10^8 times smaller than the amplitude for (b).

The approach to the isotropic diffusion limit is shown in Figure 8. The angular dependencies of the three modes of intensity are shown at various nondimensional depths in this non-absorbing medium. The homogeneous boundary condition at the surface which allows for no downward intensity is explicitly seen at $\tau = 0$. The horizontal line at each depth is the $\mu = 0$ reference line. It is included so that the backward or forward tendency of the intensity is apparent. When a nondimensional depth of 5 is reached the intensity fields are nearly isotropic and have the relation given in Eq. (118) thus verifying the numerics. For low frequencies, the longitudinal wave scattering is predominantly backscatter (see Fig. 7). This backscatter dominance is also evidenced by the large I_L lobe above the $\mu = 0$ line in Figure 8 for $k_T a = 0.1$. The forward scattering dominance at $k_T a = 3.0$ is also seen at shallow depths. The numerical values of the intensities in the diffusion limit are quite different for the two frequencies. This difference is the result of the variation in the ratio of the longitudinal scattering cross section to transverse scattering cross section with frequency. At lower frequencies this ratio is smaller allowing more of the incident energy to penetrate deeper into the medium.

When absorption is added to the medium the approach to the singly scattered solution can be observed. Figure 9 shows the outward intensity at the surface as a function of direction for

the full solution and for the singly scattered solution, both for the case of no absorption. In this case the full solution differs markedly from that of the singly scattered thus displaying the high amount of multiple scattering occurring. The intensity peak for I_{SV} at 50° for the full solution does not coincide with that of the I_{SV} peak in the singly scattered solution at 60°. Thus the multiple scattering has shifted this angular peak. When a moderate amount of absorption is added to the medium ($\tilde{\upsilon}_T = 0.111$) the qualitative nature of the full solution is more similar to the singly scattered solution as shown in Figure 10. However, the quantitative difference is still quite large. When a large amount of absorption is introduced ($\tilde{\upsilon}_T = 4$) as shown in Figure 11 the convergence of the two solutions is apparent.

At higher frequencies ($k_T a = 3.0$) the effect of the forward scattering can be seen. The outward surface intensity for this frequency can be seen in Figures 12 and 13 for no absorption and moderate absorption ($\tilde{\upsilon}_T = 0.111$), respectively.

An experiment to measure the angular dependence of the intensity may not be convenient. Alternatively, we can examine the outward backscattered intensity normal to the surface as a function of ultrasonic frequency, ω. This type of measurement is made quite frequently for polycrystalline microstructural characterization[14,16]. Figure 14 depicts the backscattered longitudinal intensity for 5 different nondimensional transverse absorption rates. A spline fit has been used to smooth the data over the frequency range. For the frequency band shown, $k_T a$ = 0.1-4.0, a peak in the longitudinal backscattered intensity is observed at around $k_T a = 1.75$ for all non-zero absorption levels. This type of information could possibly be used for experimentally determining nominal scatterer size.

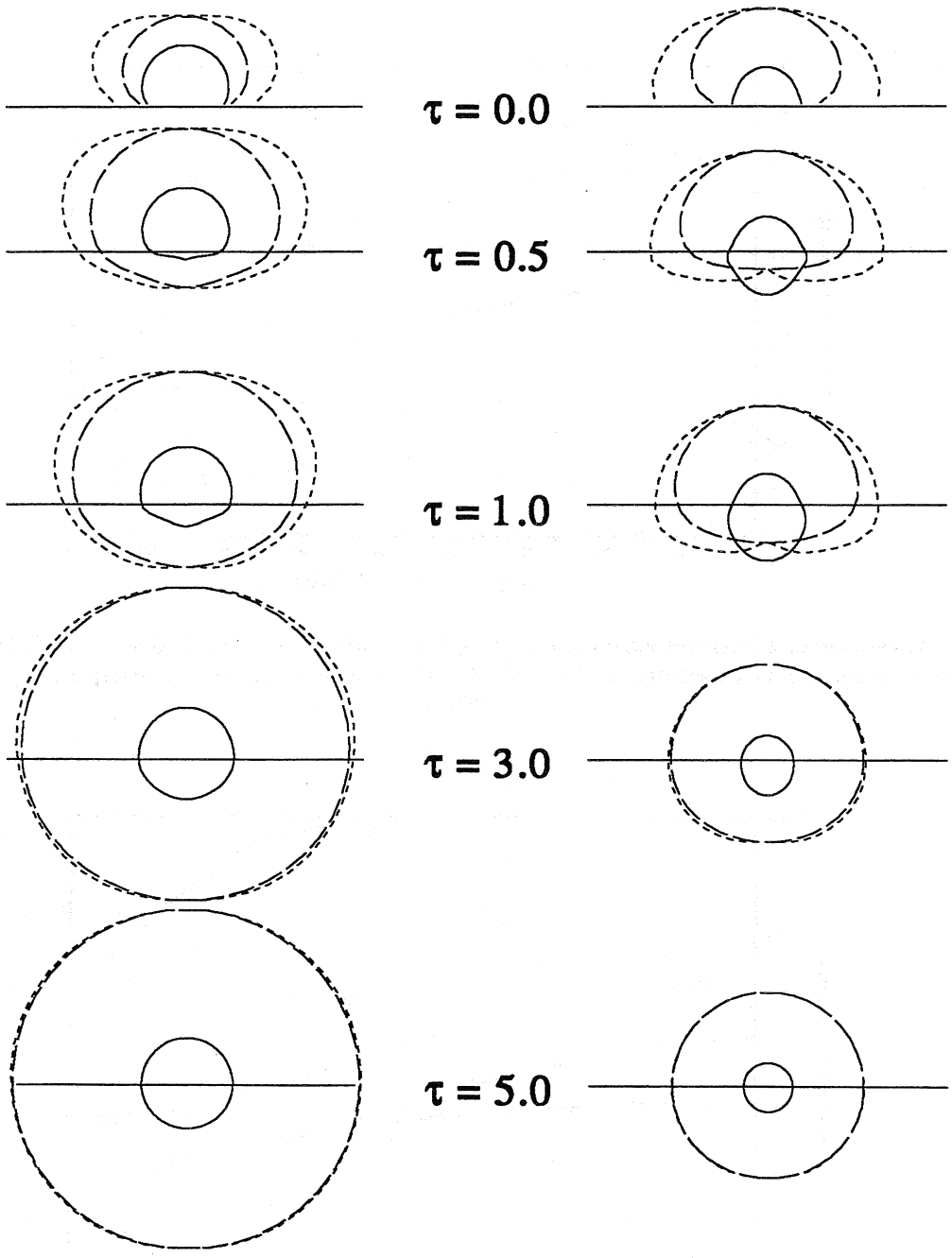

Figure 8. Angular intensity variation as a function of nondimensional depth for a normally incident longitudinal wave at two frequencies (a: $k_T a = 0.1$, b: $k_T a = 3.0$) without absorption for the three modes I_L (solid line), I_{SV} (small dash), and I_{SH} (large dash).

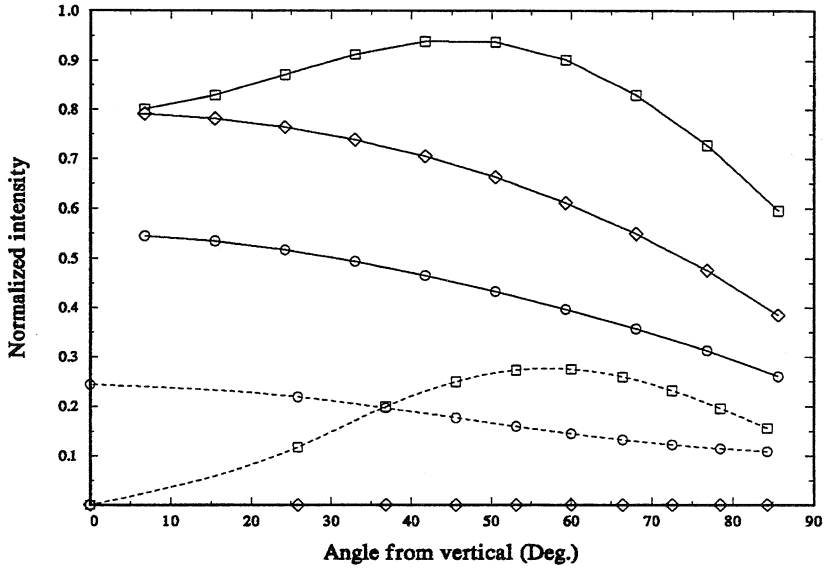

Figure 9. Outward surface intensity without absorption for $k_T a = 0.1$. The full solution is denoted by the solid lines and the singly scattered solution by the dashed lines for the three modes I_L (circle), I_{SV} (square), I_{SH} (triangle).

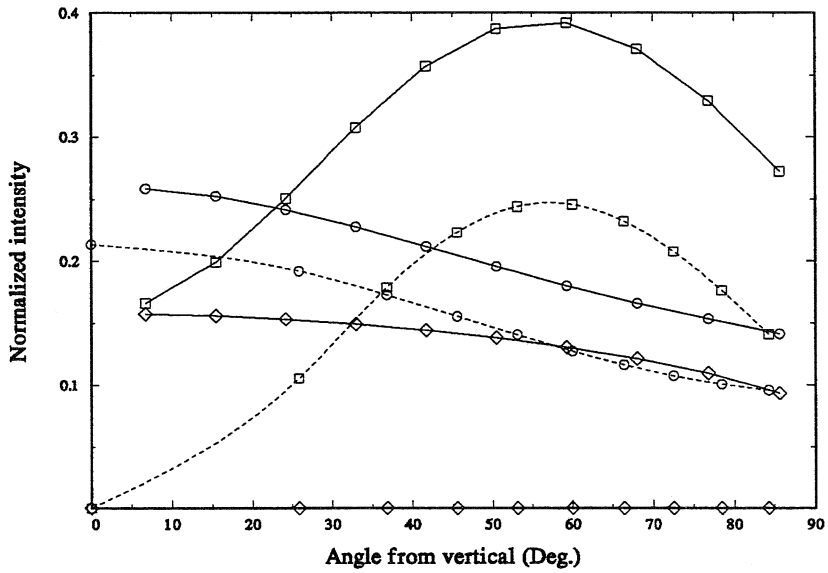

Figure 10. Outward surface intensity with moderate absorption ($\tilde{\upsilon}_T = 0.111$) for $k_T a = 0.1$. Line styles and symbols are as in Figure 9.

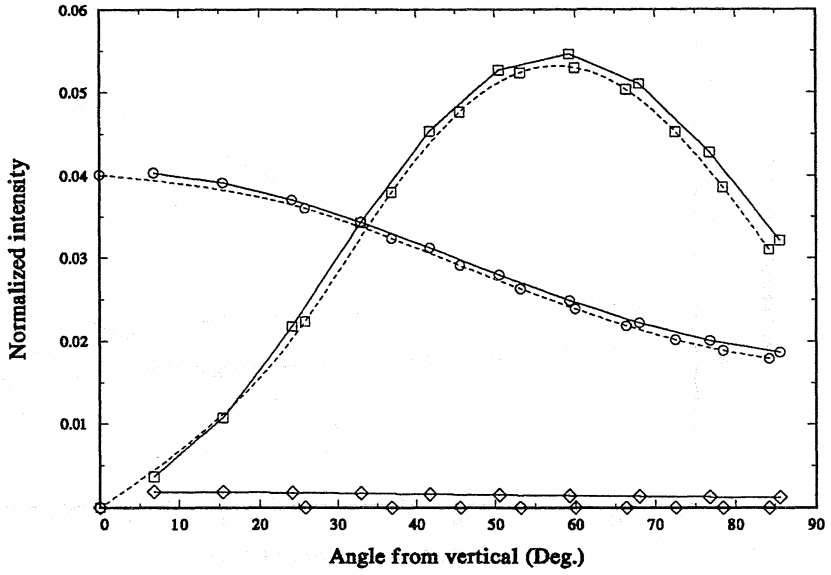

Figure 11. Outward surface intensity with high absorption ($\tilde{\upsilon}_T = 4$) for $k_T a = 0.1$. Line styles and symbols are as in Figure 9.

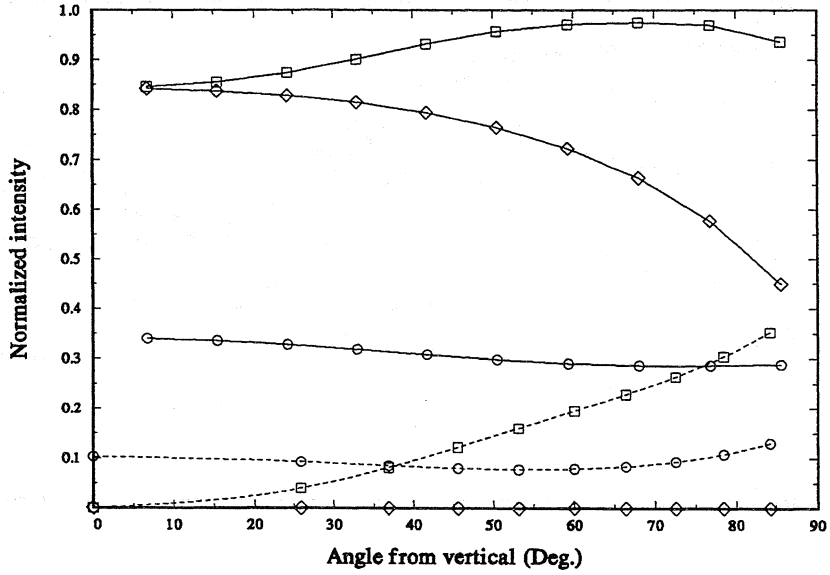

Figure 12. Outward surface intensity without absorption for $k_T a = 3.0$. Line styles and symbols are as in Figure 9.

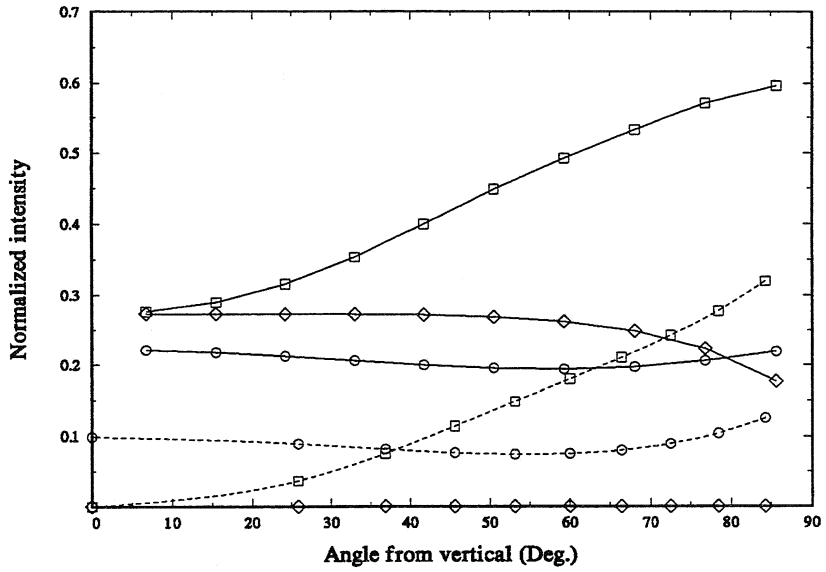

Figure 13. Outward surface intensity with moderate absorption ($\tilde{\upsilon}_T = 0.111$) for $k_T a = 3.0$. Line styles and symbols are as in Figure 9.

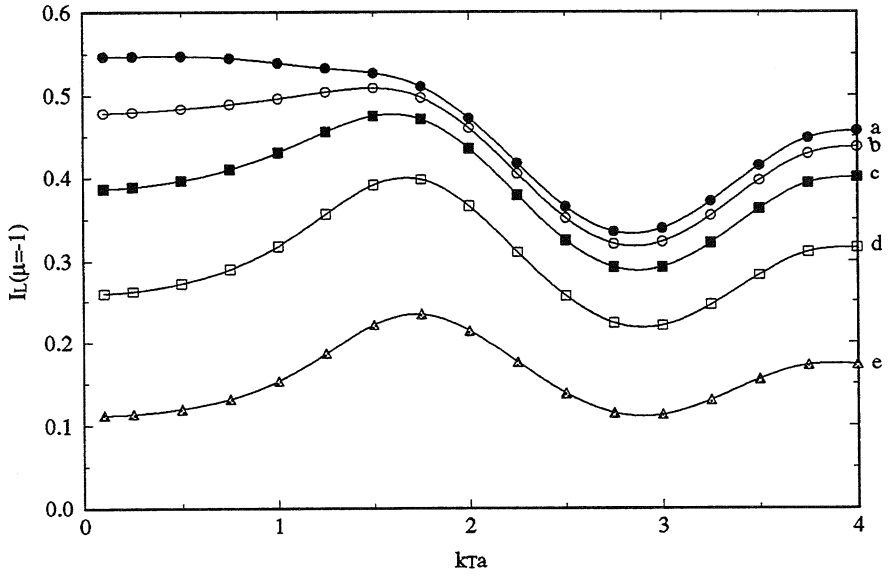

Figure 14. Longitudinal backscattered ($\mu = -1$) intensity for a normally incident longitudinal wave at five absorption rates: a) no absorption, b) $\tilde{\upsilon}_T = 0.001$, c) $\tilde{\upsilon}_T = 0.0101$, d) $\tilde{\upsilon}_T = .111$, e) $\tilde{\upsilon}_T = 1$.

B. Two Incoherent, Orthogonally Polarized, Transverse Waves Normally Incident

Axisymmetric cases (m=0 only) for incident shear waves can also be examined. Electromagnetic researchers often examine normally incident circularly polarized light in which $I_{SV0} = I_{SH0} = 1/2$, $U=0$, and $V = \pm 1$ with the sign dependent upon the sense of the circular polarization of the incident field. Another axisymmetric case is that of two orthogonal incoherent transverse waves at normal incidence in which $I_{SV0} = I_{SH0} = 1/2$, and $U=V=0$. This case is analogous to that of ''natural light'' in electromagnetic waves. For this case $\underline{S}_{L0} = 0$ and assuming unit intensity of the incident field

$$\underline{S}_{T0} = \frac{1}{8\kappa_T} \begin{Bmatrix} P_{12,0}(\mu, \mu_0 = 1) + P_{13,0}(\mu, \mu_0 = 1) \\ P_{22,0}(\mu, \mu_0 = 1) + P_{23,0}(\mu, \mu_0 = 1) \\ P_{32,0}(\mu, \mu_0 = 1) + P_{33,0}(\mu, \mu_0 = 1) \\ 0 \\ 0 \end{Bmatrix}, \tag{121}$$

where $P_{ij,0}$ is given in Eq. (120).

Polar plots can be made for the diffuse intensity in this case also. The depth dependent nature of the intensity is seen in Figure 15, drawn at the same scale as Figure 8. The approach to the diffusion limit is also seen for this case. Again the low frequency case has the expected backscatter dominance and the high frequency case the forward scatter dominance. The lobed nature of the scattering for the shear-shear modes is apparent for the higher frequency. Also a much smaller backscattered longitudinal intensity is seen for this type of incident field.

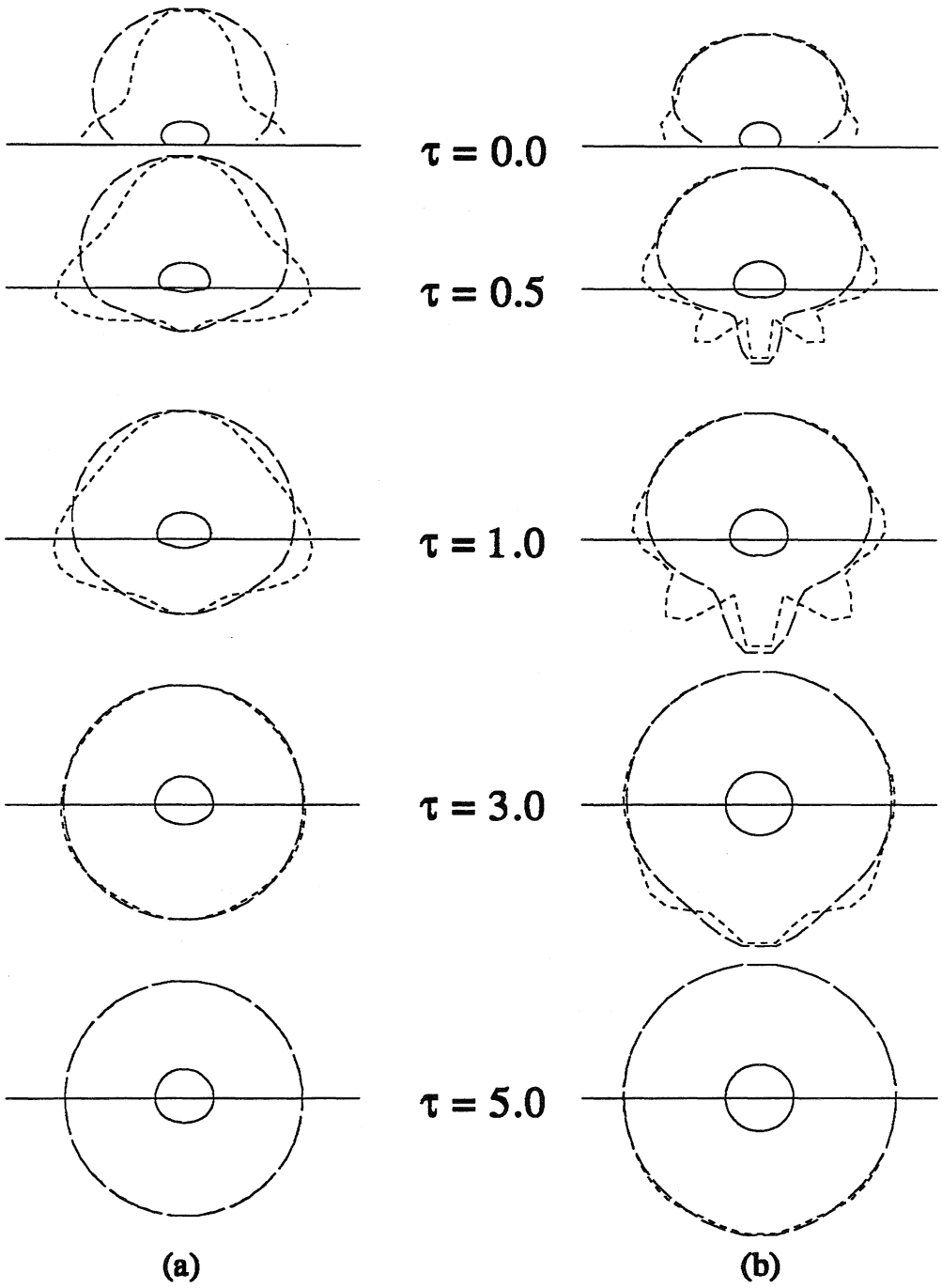

Figure 15. Angular intensity variation as a function of nondimensional depth for two normally incident orthogonally polarized transverse waves at two frequencies (a: $k_T a = 0.1$, b: $k_T a = 3.0$) without absorption for the three modes I_L (solid line), I_{SV} (small dash), and I_{SH} (large dash).

C. Discussion

The results presented above serve mainly to illustrate the robustness and plausibility of simple URTE calculations. It may well be that practical applications of the URTE and its solutions will demand solutions in the time domain, and solutions for incident fields with significant x and y dependence. Towards that end we note here that the URTE given in Eq. (25) is invariant under translations in x, y, and t and so Fourier transforms (or Hankel transforms in an axisymmetric case) provide potentially viable approaches. One anticipates fairly smooth dependencies on x, y, and t and so a small number of Fourier components may suffice. In the case of a medium with statistical inhomogeneity, one may be forced to solve the URTE using finite elements.

The current results are also confined to the case of mono-dispersed discrete spherical scatterers. The URTE is derived elsewhere for the more important NDE case of a polycrystal[40]. We anticipate a polycrystalline URTE with essentially the same structure as Eq. (25).

V. CONCLUSIONS

A radiative transfer equation has been derived for elastic waves in a scattering and absorbing medium containing discrete uncorrelated scatterers. Results have been presented for a semi-infinite medium containing randomly distributed spherical voids illuminated by steady-state plane waves at normal incidence.

The ultrasonic radiative transfer equation governs the longitudinal and both transverse diffuse intensities over the entire multiple scattering regime from single scattering to the diffusion limit. It thus contains materials information unavailable to previous single scattering theories. Therefore this approach is expected to have much wider applicability to materials characterization of random media and increase our understanding of the ultrasonic multiple scattering process.

Experimental corroboration of this theory is a next logical step. Current experimental work with diffuse intensity, used to corroborate single scattering theories, is usually conducted at normal incidence in a water bath in either the time or frequency domain. One can envision similar experiments within the context of the present theory. Comparisons with such experiments will require solutions of the present equations in more complicated geometries. One particularly notes the importance of modeling liquid-solid interface effects and obtaining solutions in the time domain. Such extensions are not likely to be difficult.

Ultrasonic radiative transfer theory has potential applications in a variety of materials characterization problems including ones in polycrystalline metals, concrete, geophysical media, composite materials and other random media where scattering effects are important.

ACKNOWLEDGEMENT

This work was sponsored by the National Science Foundation, Grant No. MSS-91-14360.

REFERENCES

1. W. P. Mason and H. J. McSkimm, "Attenuation and scattering of high frequency sound waves in metals and glasses," *J. Acoust. Soc. Am.* **19**, 464-473 (1947).

2. A. B. Bhatia, "Scattering of high-frequency sound waves in polycrystalline materials," *J. Acoust. Soc. Am.* **19**, 16-23 (1959A).

3. E. P. Papadakis, "Scattering in polycrystalline media," *Meth. Exp. Phys.* **19**, 237-298 (1981).

4. D. W. Fitting and L. Adler, *Ultrasonic Spectral Analysis for Nondestructive Evaluation*, Plenum, New York, 1981.

5. A. Vary, "Ultrasonic measurement of material properties," *Research Techniques in Nondestructive Testing V. IV*, ed. R. S. Sharpe, Academic Press, 1980.

6. F. E. Stanke and G. S. Kino, "A unified theory for elastic wave propagation in polycrystalline materials," *J. Acoust. Soc. Am.* **75**, 665-681 (1984).

7. S. Hirsekorn, "The scattering of ultrasonic waves by polycrystals," *J. Acoust. Soc. Am.* **72**, 1021-1031 (1982).

8. V. Twersky, "Coherent scalar field in pair-correlated random distributions of aligned scatterers," *J. Math. Phys.* **18**, 2468-2486 (1977).

9. L. Tsang, J. A. Kong, and T. Habashy, "Multiple scattering of acoustic waves by random distribution of discrete spherical scatterers with the quasicrystalline and Percus-Yevick approximation," *J. Acoust. Soc. Am.* **71**, 552-558 (1982).

10. V. K. Varadan, Y. Ma, and V. V. Varadan "A multiple scattering theory for elastic wave propagation in discrete random media," *J. Acoust. Soc. Am.* **77**, 375-385 (1985).

11. J. Saniie and N. M. Bilgutay, "Quantitative grain size evaluation using ultrasonic backscattered echoes," *J. Acoust. Soc. Am.* **80**, 1816-1824 (1986).

12. B. Fay, "Theoretical considerations of ultrasound backscatter," (in German) *Acustica* **28**, 354-357 (1973).

13. K. Goebbels, "Ultrasonics for microcrystalline structure examination," *Phil. Trans. R. Soc. Lond. A* **320**, 161-169 (1986).

14. F. J. Margetan, T. A. Gray, and R. B. Thompson, "A technique for quantitatively measuring microstructurally induced ultrasonic noise," *Review of Progress in Quantitative NDE, 10*, D. O. Thompson and D. E. Chimenti, Eds., Plenum Press, New York, 1721-1728 (1991).

15. J. H. Rose, "Ultrasonic backscatter from microstructure," *Review of Progress in Quantitative NDE, 11*, D. O. Thompson and D. E. Chimenti, Eds., Plenum Press, New York, 1677-1684 (1992).

16. M. D. Russell and S. P. Neal, "Grain noise power spectrum estimation for normal incidence ultrasonic interrogation of weak scattering polycrystalline materials using experimentally estimated longitudinal-wave backscatter coefficients," to be published in *Ultrasonics*.

17. C. B. Guo, P. Holler, and K. Goebbels, "Scattering of ultrasonic waves in anisotropic polycrystalline metals," *Acustica* **59**, 112-120 (1985).

18. R. L. Weaver, "Diffusivity of ultrasound in polycrystals," *J. Mech. Phys. Solids* **38**, 55-86 (1990).

19. R. L. Weaver, W. Sachse, K. Green, and Y. Zhang, "Diffuse ultrasound in polycrystalline solids," Proceedings of Ultrasonics International, Le Touquet, France, July, 1991.

20. K. Goebbels, "Structure analysis by scattered ultrasonic radiation," *Research Techniques in Nondestructive Testing V. IV*, ed. R. S. Sharpe, Academic Press, 1980.

21. S. Chandrasekhar, *Radiative Transfer*, Dover, New York, 1960.

22. V. V. Sobolev, *A Treatise on Radiative Transfer*, D. Van Nostrand, New Jersey, 1963.

23. A. Ishimaru, *Wave Propagation and Scattering in Random Media*, Vol. 1, Academic Press, New York, 1978.

24. In the limit that scattering per wavelength is extremely strong, with attenuations per wavelength on the order of the wavenumber, it is interesting to note that residual phase coherence in the multiply scattered wave may lead to striking deviations[16] from the predictions of radiative transfer theory. These deviations, however, are known to occur only at scattering strengths which are very hard to achieve in practice.

25. Y. N. Barabanenkov and V. M. Finkel'berg, "Radiation transport equation for correlated scatterers," *Zh. Eksp. Teor. Fiz.* **53**, 978-986 (1967) [*Sov. Phys. - JETP* **26**, 587-591 (1968)].

26. H. C. van de Hulst, *Light Scattering by Small Particles*, Dover, New York, 1981.

27. V. Kourganoff, *Basic Methods in Transfer Problems - Radiative Equilibrium and Neutron Diffusion*, Dover, New York, 1963.

28. G. G. Stokes, "On the composition and resolution of streams of polarized light from different sources," *Trans. Camb. Phil. Soc.* **IX**, p. 399 (1852).

29. A. Ishimaru and R. L. Cheung, "Transmission, backscattering, and depolarization of waves in randomly distributed spherical particles" *Appl. Optics*, **21**, (1982).

30. G. Mie, "Beiträge zur Optik trüber Medien, speziell kolloidaler Metallösungen," *Ann. Physik*, **330**, 377-445 (1908).

31. C. F. Ying and R. Truell, "Scattering of a plane longitudinal wave by a spherical obstacle in an isotropically elastic solid," *J. Appl. Phys.* **27**, 1086-1097 (1956).

32. N. G. Einspruch, E. J. Witterholt, and R. Truell, "Scattering of a plane transverse wave by a spherical obstacle in an elastic medium," *J. Appl. Phys.* **31**, 806-818 (1960).

33. D. Deirmendjian, *Electromagnetic Scattering on Spherical Polydispersions*, American Elsevier, New York, 1969.

34. Z. Sekera, "Scattering matrices and reciprocity relationships for various representations of the state of polarization," *J. Opt. Soc. Am.* **56**, 1732-1740 (1966).

35. J. D. Achenbach, *Wave Propagation in Elastic Solids*, Elsevier, New York, 1984.

36. R. L. Weaver, "On diffuse waves in solid media," *J. Acoust. Soc. Am.* **71**, 1608-1609 (1982).

37. W. E. Boyce and R. C. DiPrima, *Elementary Differential Equations and Boundary Value Problems*, Wiley, New York, 1977.

38. P. M. Morse and H. Feshbach, *Methods of Theoretical Physics*, McGraw Hill, New York, 1953.

39. J. W. Hovenier, "Symmetry relationships for scattering of polarized light in a slab of randomly oriented particles," *J. Atmos. Sci.* **26**, 488-499 (1969).

40. J. A. Turner and R. L. Weaver, "Radiative transfer and multiple scattering of diffuse ultrasound in polycrystalline media," in preparation.

List of Recent TAM Reports

No.	Authors	Title	Date
499	Cardenas, H. E., W. C. Crone, D. J. Scott, G. G. Stewart, and B. F. Tatting	Twenty-sixth student symposium on engineering mechanics, M. E. Clark, coord. (1989)	Mar. 1992
700	Juister, C. E., D. W. Newport, C. S. Payne, J. M. Peters, M. P. Thomas, and J. C. Trovillion	Twenty-seventh student symposium on engineering mechanics, M. E. Clark, coord. (1990)	Apr. 1992
701	Bernard, R. T., D. W. Claxon, J. A. Jones, V. R. Nitzsche, and M. T. Stadtherr	Twenty-eighth student symposium on engineering mechanics, M. E. Clark, coord. (1991)	Apr. 1992
702	Greening, L. E., P. J. Joyce, S. G. Martensen, M. D. Morley, J. M. Ockers, M. D. Taylor, and P. J. Walsh	Twenty-ninth student symposium on engineering mechanics, J. W. Phillips, coord. (1992)	May 1992
703	Kuah, H. T., and D. N. Riahi	Instabilities and transition to chaos in plane wakes	Nov. 1992
704	Stewart, D. S., K. Prasad, and B. W. Asay	Simplified modeling of transition to detonation in porous energetic materials	Nov. 1992
705	Stewart, D. S., and J. B. Bdzil	Asymptotics and multi-scale simulation in a numerical combustion laboratory	Jan. 1993
706	Hsia, K. J., Y.-B. Xin, and L. Lin	Numerical simulation of semi-crystalline Nylon 6: Elastic constants of crystalline and amorphous parts	Jan. 1993
707	Hsia, K. J., and J. Q. Huang	Curvature effects on compressive failure strength of long fiber composite laminates	Jan. 1993
708	Jog, C. S., R. B. Haber, and M. P. Bendsoe	Topology design with optimized, self-adaptive materials	Mar. 1993
709	Barkey, M. E., D. F. Socie, and K. J. Hsia	A yield surface approach to the estimation of notch strains for proportional and nonproportional cyclic loading	Apr. 1993
710	Feldsien, T. M., A. D. Friend, G. S. Gehner, T. D. McCoy, K. V. Remmert, D. L. Riedl, P. L. Scheiberle, and J. W. Wu	Thirtieth student symposium on engineering mechanics, J. W. Phillips, coord. (1993)	Apr. 1993
711	Weaver, R. L.	Anderson localization in the time domain: Numerical studies of waves in two-dimensional disordered media	Apr. 1993
712	Cherukuri, H. P., and T. G. Shawki	An energy-based localization theory: Part I—Basic framework	Apr. 1993
713	Manring, N. D., and R. E. Johnson	Modeling a variable-displacement pump	June 1993
714	Birnbaum, H. K., and P. Sofronis	Hydrogen-enhanced localized plasticity—A mechanism for hydrogen-related fracture	July 1993
715	Balachandar, S., and M. R. Malik	Inviscid instability of streamwise corner flow	July 1993
716	Sofronis, P.	Linearized hydrogen elasticity	July 1993
717	Nitzsche, V. R., and K. J. Hsia	Modelling of dislocation mobility controlled brittle-to-ductile transition	July 1993
718	Hsia, K. J., and A. S. Argon	Experimental study of the mechanisms of brittle-to-ductile transition of cleavage fracture in silicon single crystals	July 1993
719	Cherukuri, H. P., and T. G. Shawki	An energy-based localization theory: Part II—Effects of the diffusion, inertia and dissipation numbers	Aug. 1993
720	Aref, H., and S. W. Jones	Chaotic motion of a solid through ideal fluid	Aug. 1993
721	Stewart, D. S.	Lectures on detonation physics: Introduction to the theory of detonation shock dynamics	Aug. 1993
722	Lawrence, C. J., and R. Mei	Long-time behavior of the drag on a body in impulsive motion	Sept. 1993
723	Mei, R., J. F. Klausner, and C. J. Lawrence	A note on the history force on a spherical bubble at finite Reynolds number	Sept. 1993
724	Qi, Q., R. E. Johnson, and J. G. Harris	A re-examination of the boundary layer attenuation and acoustic streaming accompanying plane wave propagation in a circular tube	Sept. 1993
725	Turner, J. A., and R. L. Weaver	Radiative transfer of ultrasound	Sept. 1993